One gene - two proteins: The C-terminus of the prototypical M2 muscarinic receptor localizes to the mitochondria

Irene Fasciani[1†], Francesco Petragnano[1†], Ziming Wang[2], Ruairidh Edwards[3], Narasimha Telegu[2], Ilaria Pietrantoni[1], Henrik Zauber[2], Mario Rossi[3], Ulrike Zabel[4], Marlies Grieben[2], Maria E. Terzenidou[3], Jacopo Di Gregorio[1], Cristina Pellegrini[1], Silvano Santini Jr[5], Anna R. Taddei[6], Barbel Pöhl[2], Stefano Aringhieri[7], Marco Carli[7], Gabriella Aloisi[1], Francesco Marampon[8], Alexandra Roman[2], Sebastian Diecke[2], Vincenzo Flati[1], Franco Giorgi[7], Fernanda Amicarelli[5], Andrew B. Tobin[3], Marco Scarselli[7], Kostas Tokatlidis[3], Martin J. Lohse[2,4,9]*, Roberto Maggio[1]*, Paolo Annibale[2,10]*

[1] Department of Biotechnological and Applied Clinical Sciences, University of L'Aquila, 67100 L'Aquila, Italy.
[2]Max Delbrück Center for Molecular Medicine, 13125 Berlin, Germany.
[3]Centre for Translational Pharmacology, Institute of Molecular, Cell and Systems Biology, College of Medical, Veterinary and Life Sciences, University of Glasgow, G128QQ Glasgow, UK.
[4]Institute of Pharmacology and Toxicology, University of Würzburg, 97078 Würzburg, Germany.
[5]Department of Life, Health and Environmental Sciences, University of L'Aquila, 67100 L'Aquila, Italy.
[6]Section of Electron Microscopy, Great Equipment Center, University of Tuscia, Viterbo, Italy.
[7]Department of Translational Research and New Technology in Medicine, University of Pisa, 56126 Pisa, Italy.
[8]Department of Radiotherapy, University of Roma La Sapienza, 00151 Roma, Italy.
[9]ISAR Bioscience Institute, 82152 Munich, Germany.
[10]School of Physics and Astronomy, University of St Andrews, KY16 9SS St Andrews.
[†] Equal contribution
*email: m.lohse@mdc-berlin.de;
*email: roberto.maggio@univaq.it;
*email: paolo.annibale@mdc-berlin.de

Abstract

Muscarinic acetylcholine receptors are G protein-coupled receptors activated by the endogenous neurotransmitter acetylcholine. We show here that the carboxyl terminal fragment of the muscarinic M_2 receptor, containing the transmembrane regions 6 and 7 (M_2tail), is expressed by virtue of an internal ribosome entry site. Radioligand binding, biochemical and molecular biology experiments, combined to advanced fluorescence microscopy reveal that the M_2tail, whose expression is upregulated in cells undergoing integrated stress response, does not follow the normal route to the plasma membrane, but is almost exclusively sorted to the mitochondria inner membrane: here it controls oxygen consumption, cell proliferation and the formation of ROS by reducing oxidative phosphorylation. Genetic editing of the key methionine where cap-independent translation occurs, reveals the physiological role of this process in influencing cell proliferation and oxygen consumption. The expression of the C-terminal of a GPCR, capable of regulating mitochondrial function, constitutes a hitherto unknown mechanism that cells may use for controlling their metabolism under variable environmental conditions, notably unrelated to the canonical signalling function of the GPCR at the plasma membrane.

Teaser

A G protein-coupled receptor fragment localizing in the mitochondria unexpectedly links two hitherto unrelated aspects of cell biology.

Introduction

Muscarinic receptors include five structurally related receptors, belonging to class A of the G protein-coupled receptor (GPCR) family (1). They are comprised of seven trans-membrane domains (TM domains 1-7) connected by intra and extracellular loops. Of these structural elements, the third intracellular (i3) domain is the one conferring a coupling specificity for G proteins, β-arrestin recruitment and endocytic internalization (2). However, only a small portion of the i3 loop is required for receptor function, and for this reason large deletions of this segment have no effect on receptor activation and internalization (3).

We could previously show that the M_2 receptor can be split at the level of the i3 loop into two segments, each behaving as an autonomous folding unit capable of targeting the plasma membrane and surprisingly reconstituting a physiologically active receptor when expressed together in transfected cells (4). In the context of these studies, a mutant of the receptor carrying a stop codon in position 228 was surprisingly observed to retain (albeit reduced) ligand binding in radioligand binding assays (11). This finding cannot be explained by the fact that the insertion of the stop codon results in the expression of an N-terminal receptor fragment, constituted by the TM regions 1-5, since this fragment alone has been shown to be not able to bind muscarinic ligands and to trigger signal transduction (12). Therefore, an alternative explanation for the behavior of stop-codon mutant 228 is needed. Since the N-terminal fragment can reconstitute a physiologically active receptor when co-transfected with the C-terminal fragment, a plausible possibility is that the C-terminal segment of the receptor can be independently produced and reconstitute an active receptor with the N-terminal portion on the cell membrane. This scenario opens the interesting question of how the C-terminal fragment can be translated endogenously as an independent polypeptide.

In eukaryotes, the most common mechanism of translation initiation is the cap-dependent process, which requires the interaction of several key proteins at the 5'-end (5′ cap) of mRNA molecules. However, in recent years, it has been demonstrated that the presence of internal ribosome entry site (IRES) sequences, which are common features of virus replication (5), can mediate cap independent translation of eukaryotic RNA(s) (6). This presents the suggestive possibility that a cap-independent translation of the M_2 C-terminal domain indeed occurs in this mutant, opening a number of important questions about the molecular processes involved in the synthesis and subcellular behaviour of the C-terminal domain fragment.

GPCRs are normally distributed at the plasma membrane, where, after activation by an agonist and coupling to G proteins, regulate a number of intracellular effectors. Nevertheless, non-canonical localizations of GPCRs have also been described, such as in endosomes (7), cell division compartments (centrosomes, spindle midzone and midbodies) (8), and mitochondria (9,10), underpinning non-traditional roles for this protein family.

In this work, we therefore set out to explore whether the expression of the C-terminal domain of the M_2 muscarinic receptor, a region containing the TM regions 6 and 7, occurs naturally by a cap-independent translation mechanism. Combining radio-ligand binding, molecular biology approaches, advanced fluorescence imaging and genetic editing of human induced pluripotent stem cells (hiPSCs) we have observed that the C-terminal domain of this receptor is indeed expressed as an independent polypeptide. Surprisingly, using bimolecular fluorescence complementation, in-vitro mitochondrial import assays and cell metabolism assays we observe that the C-terminal domain is strongly targeted to the cell mitochondria. Importantly, this mitochondrial targeting has functional ramifications since both cap-dependent mediated overexpression of the C-terminal domain alone, as well as cap-independent mediated translation starting from the mRNA of the full length M_2 receptor, resulted in a sizable reduction of oxidative phosphorylation. In summary, our study reports the new observation that alternative reading of a GPCR receptor gene can translate into a fragment of the receptor that serves a cellular function entirely different from canonical GPCR signalling.

Results

Ligand binding and functional properties of M_2 receptors mutants

To investigate and distinguish the functional roles of the two known N-terminal (TM1-5) and C-terminal (TM6-7) domains of the M_2 muscarinic receptor, we expressed C-terminally truncated variants of the receptor in COS-7 cells. We first observed that the M_2stop228 construct, a receptor mutant bearing a stop codon at the beginning of the i3 loop in position 228 (but containing the downstream sequence, i.e. leading to the transcription of an mRNA of the same length as that of the wt M_2R) (**Fig. 1a** and **Fig. S1**), exhibited unexpected binding activity (11) albeit at a very low level of expression, i.e. 45 fmol/mg of protein. Both K_D value of [^{3}H]NMS (N-methylscopolamine, an antagonist) calculated from direct saturation experiments, and the IC_{50} values, calculated in competition experiments for the agonist carbachol, were in fact similar to those calculated for the wild type M_2 receptor (**Table 1**). Furthermore, the M_2stop228 receptor was found functionally active as it was capable to inhibit adenylyl cyclase (11) and increase ERK phosphorylation (**Fig.**

S2b), even though the extent of response was reduced if compared to the wild type M_2 receptor. On the other hand, if a stop codon is inserted upstream or downstream of position 228, e.g. at positions 196 or 400, no radioligand binding can be observed (**Fig. 1a** and **Table S1**).

As we demonstrated in an earlier report (12), another receptor fragment whose sequence runs only until position 283 (i.e. comprising only TM1-5) of the corresponding wt receptor, called M_2trunk(1-283) (**Fig. S1**), did not show any radio-ligand binding activity upon expression in COS-7 cells, despite comprising the first five trans-membrane regions of the wild type M_2 receptor, as the M_2stop228 construct (**Table 1**). Consistently, a construct containing only the M_2 receptor sequence until amino acid 228 (M_2trunk(1-228)), did not show any radio-ligand binding (**Table 1**).

On the other hand, we observed binding and downstream signaling ability in co-transfection experiments of the M_2trunk(1-283) and M_2tail(281-466) (**Table 1**), the latter being a construct containing only the sequence between aminoacid 368 and the end of the M_2 receptor, i.e. comprising TM6 and 7. Therefore, co-expression of the M_2trunk(1-283) (TM1-5) and M_2tail(368-466) (TM6-7) reconstitutes a functional full length receptor at the cell membrane (**Fig. 1b**).

These data suggest that, for the M_2stop228 receptor to display binding and functional activity, the receptor sequence downstream of the stop codon in position 228 (containing TM6 and 7) has (i) to be translated and (ii) to presumably interact with the first five TM regions of the M_2 receptor. This notion is graphically summarized in **Fig. 1b.** For this hypothesis to be true, however, the C-terminal portion of the receptor needs to be expressed despite the presence of stop codons in the i3 loop in our M_2stop228 mutant. Indeed, we confirmed expression of the C-terminal fragment by fusing an enhanced Green Fluorescent Protein (EGFP) at the C terminus of several receptor mutants (**Fig. 1c**).

Interestingly, though, while cells expressing the M_2-EGFP displayed the normal, predominant plasma membrane expression (**Fig. 1c**), cells expressing the M_2stop228-EGFP displayed a visible intracellular green fluorescence, which is in stark contrast to cells expressing M_2stop400-EGFP, which do not show any fluorescence, in line with the non-transfected control.

To further analyze the atypical behavior of M_2stop228-EGFP, which by displaying green fluorescence confirms that the sequence downstream of the stop in position 228 is indeed translated, we generated a frame shift mutant: we inserted a single guanine nucleotide in the sequence of the M_2-EGFP, changing the

methionine in position 368 into an aspartate, which in turn generates an in-frame stop codon at position 370. We named the construct, which notably still displays an EGFP signal in transfected cells, M_2fr.sh.-EGFP (**Fig. 1c**). The observation that the mutant retains EGFP fluorescence is most remarkable, since the EGFP is now out of the original reading frame and it can only be properly translated by a cap-independent translation mechanism, starting from a methionine in the new reading frame.

Furthermore, the observation that both M_2stop228-EGFP and M_2fr.sh.-EGFP retain EGFP fluorescence, whereas M_2stop400-EGFP does not, indicates not only that a cap independent translation mechanism occurs, but also that the starting methionine for the process must be downstream of stop 228 and upstream of stop 400, leaving as a leading candidate the third in-frame methionine of the i3 loop. This is in line with the radio-ligand binding data from co-expression of receptor mutants carrying a double stop codon, the first in position 228 and the second in positions ranging from 248 to 400, including mutations of the first (M248) and second (M296) in-frame methionines in the third i3 loop (**Fig. S1**, **Fig. 1a** and **Fig. S2a**), further pointing to M368 as the most likely site for the cap-independent initiation of translation of the C-terminal domain.

Immunodetection of the M_2 carboxyl terminal fragment

To further characterize the expression of the C-terminal fragment and verify the hypothesis of cap-independent translation, we tagged several of the M_2 receptors mutants described above with a myc-tag for immune detection. The constructs were subcloned in a bicistronic vector backbone, allowing also the expression of the red fluorescent protein mRuby2 as a fluorescent reporter, in order to verify comparable expression levels. HEK293 cells were therefore transfected with the wild type M_2 receptor M_2-myc, the C-terminal fragment starting at the third in-frame methionine M_2tail(368-466)-myc, a mutant of the M_2 receptor with the third in-frame methionine mutated to an alanine, M_2M368A-myc that as discussed above should affect the cap-independent translation, and finally the M_2stop400-myc; the constructs were resolved by SDS-PAGE and assayed by Western blotting, as displayed in **Fig. 2a**. Based on the amino acid sequence, the expected molecular weights for the full length receptor and the C-terminal fragment (inclusive of the myc tag) are ~75 kDa and below ~20 kDa respectively.

Interestingly, M_2tail(368-466) runs with two clear bands ~22 and ~15 kDa (**Fig. 2a**), indicating the presence of post-translational modifications and protein processing (see **Discussion)** and thus defining the qualitative

pattern expected for the M_2 carboxyl terminal fragment starting at the third in-frame start codon (M368). The full-length receptor was observed, as expected, at about ~75 kDa together with commonly observed higher order oligomers (13). Notably, the M_2 receptor clearly displays the lower MW band pair also seen for M_2tail(368-466). The strongest confirmation for a cap-independent translation process is found in the M_2M368A: here the ~20 kDa band disappears. In line with what we observed for its EGFP tagged version, the M_2stop400 does not exhibit any band, comparable to the negative control using untransfected cells. The absence of any band further excludes the possibility of a downstream cap-independent translation site yielding a fragment originating from the next in frame methionine (406) (**Fig. 2a**). Altogether these results support the notion that the band at ~20 kDa observed in the wild type M_2 receptor lane is the bona-fide tail fragment originated by a cap-independent translation mechanism, and that the origin of this process is at the third in frame methionine (M368) of the M_2 receptor.

We then tested whether a similar phenomenon, namely the translation of the C-terminal portion of the M_2 receptor, could be observed endogenously in physiological settings. We therefore prepared protein extracts from heart, brain and spleen tissues from a line of knock-in mice (see **Methods**), designed to have expression of a Chrm2/tdtomato fusion protein driven by the endogenous M_2 muscarinic acetylcholine receptor promoter/enhancer sequences. The heart and brain are known to express sizable levels of the M_2 receptor, whereas the spleen, where no expression of the M_2 receptor is reported in the proteomic databases, was used as a negative control.

The use of a transgene tag was necessary, since antibody against the M_2 receptor are notoriously ineffective, in particular when targeted at the C-terminal portion of the receptor. Instead, the tdtomato fluorescent protein can be targeted by a specific polyclonal antibody, as shown by the Western blot displayed in **Fig. 2b**. As expected, the full-length receptor-tdtomato fusion was observed at ~130 kDa (~75 kDa contributed by the receptor and ~55 kDa contributed by tdtomato).

Notably, both in the heart and brain, but not in the spleen, of these knock-in animals we observed a band doublet at ~75 kDa, which corresponds to the sum of the molecular weights of the tail fragment (~20 kDa, see above and **Fig. 2a**) and the molecular weight of tdtomato.

Testing bicistronic constructs for the presence of an IRES

To explain the translation of the carboxyl terminal fragment of the M_2 receptor, a mechanism enabling a cap-independent initiation of protein synthesis should be hypothesized (5,6). Accordingly, an IRES should be found downstream of the artificial stop codon 228 and upstream of the third in-frame methionine (codon 368) of the i3 loop. Before testing this hypothesis, we first ruled out several alternative mechanisms that could lead to the translation of M2tail, such as stop codon read-through, termination-reinitiation and alternative splicing in the translation of M2tail, as discussed in the **Supplementary Materials** and in **Fig. S3**). Then, to test the hypothesis that an IRES is leading to the cap-independent translation of the C-terminal domain, we prepared a fluorescence reporter construct in which the i3 loop of M_2 (from nucleotide 685 (a.a. 228) to nucleotide 1101 (a.a. 368)) was inserted between the two fluorescent proteins Sirius and EGFP (**Fig. 3a**). This construct, named Sirius-M_2i3(417n)-EGFP, would translate Sirius according to the classical cap-dependent mechanism, and, at the same time, it would drive EGFP translation only if the M_2i3 loop contains an IRES sequence, effectively acting as a bicistronic expression cassette. We transfected several cell lines with this construct, all positive for the blue and green fluorescence (**Fig. S4**). HEK293, used throughout our study, also appeared positive for both the blue and green fluorescence, as shown in the inset of **Fig. 3a**.

To rule out the possibility that EGFP translation from the Sirius-M_2i3(417n)-EGFP construct could be due to read-through and termination-re-initiation mechanisms, a mRNA hairpin loop was inserted in the sequence after the stop codon of the Sirius protein. The resulting construct (named Sirius-H-M_2i3(417n)-EGFP) showed only a slight reduction of the EGFP/Sirius with respect to the value measured for the analogous reporter without hairpin (~90%) (**Fig. 3a**). In contrast the Sirius-H-EGFP plasmid, where the entire M_2i3 loop after the Sirius was removed, showed a negligible EGFP/Sirius ratio (below 5%), underlining the importance of the i3 loop for EGFP expression (**Fig. 3a**). Notably, when the hairpin was inserted within the i3 loop of the full length M_2-EGFP, upstream of the M368, it was still possible to observe GFP fluorescence (**Fig. S5**).

To narrow down the position of the IRES sequence we divided the M_2 i3 loop in three parts and the resulting nucleotide sequences, 685-699, 685-1071 and 685-699/1072-1101, were inserted downstream of the hairpin loop in three different constructs (**Fig. 3a** and **Fig. S6**).

EGFP fluorescence was not significantly rescued upon insertion of the first 15 nucleotides (685-699) of the i3 loop after the hairpin, nor by the addition of the subsequent 372 nucleotides (685-1071). However, when

the last portion of the M_2 i3 loop was inserted in the construct after the Hairpin, leading to Sirius-H-M_2i3(15n/30n)-EGFP, ~110 % of the value measured for the Sirius-M_2i3(417n)-EGFP plasmid was recovered (**Fig. 3a**).

These results strongly suggest that the IRES is located in a region of the i3 loop sequence immediately upstream of the third methionine (M368) (see **Fig. 1a**), as also confirmed from ribosome profiling data from human left ventricle tissue, displaying increased p-sites as well as overall ribosomal coverage in correspondence of this region. This conclusion is further supported by the finding that when each of the three in-frame i3loop methionines (namely M248, M296 and M368) after the stop codon 228 of the M_2stop228 were mutated to an additional stop codon, only the mutation of M368 to a stop codon proved capable of completely abolishing [^{3}H]NMS binding (**Supplementary Materials** and **Fig. S1 and Table S1**). These binding results can furthermore rule out read-through and termination re-initiation: if these mechanisms were responsible for translation of the C-terminal of the M_2stop228, suppression of the first methionine would have abolished the binding. Finally, the origin of the carboxyl terminal fragment of M_2 at the third in-frame methionine (M368) is also supported by the key observation that the mutant M_2-M368A does not display the ~20 kDa band for the M_2 C-terminal fragment as compared to the wild type M_2 receptor in the Western blot of **Fig. 2a**.

Based on this evidence, we mutated the conserved residues highlighted in yellow in **Fig. S6a**, in order to check for their relevance in recruiting the ribosome on the M_2 i3 loop sequence, as shown in **Fig. 3b**. As discussed in detail in the **Supplementary Materials**, we found that the four nucleotides AAGA1090-1093 next to the methionine 368 play a pivotal role in recruiting the ribosome on the M_2 mRNA and in translating the M_2 C-terminal fragment.

Generalization to other members of the GPCR superfamily

In order to determine if the observed behavior is specific to the M_2 receptor, or could highlight a feature common to other members of the GPCR superfamily, we repeated several of our experiments in another GPCR, the related muscarinic M_3 receptor. The M_3 displays an in-frame methionine at the end of the i3loop, in position 481 (**Fig. S6a**). We then inserted a stop codon in position 273, generating the construct M_3stop273 that still displayed radio-ligand binding. Several other mutants, mimicking the single and double stop

mutations performed for the M_2 displayed a behavior consistent with M481 being the start point of a cap-independent translation of the C-terminal also for the M_3 receptor (**Table S2 and S3**), thus indicating that IRES-mediated cap-independent translation of the C-terminal domain could be a phenomenon not restricted solely to the M_2 receptor, but may be shared at least by some other members of the GPCR superfamily. The presence of an IRES sequence upstream of M481 further appears to be supported by the observation that 558 nucleotides from the i3 loop of the M_3 receptor (from nucleotide 880 to 1437) were inserted in the same Sirius-EGFP reporter construct as used for the M_2 (**Fig. S6b**). This appears to be indeed supported by the sequence-alignment of the five muscarinic receptors. The alignment of the last portion of the M_2 i3 loop (from nucleotide 1072 to 1104) with regions adjacent to the second (M_1), fourth (M_3 and M_4) and first (M_5) in-frame Methionines, clearly shows that some nucleotide residues are conserved (**Fig. S6a**). Overall these data underline that cap-independent translation could be a more general feature of GPCRs mRNAs.

Localization of the M_2 C-terminal fragment generated by cap-dependent expression under the control of a viral promoter

After having established that the expression of the M_2 C-terminal domain is regulated by an IRES and that its translation starts at M368, we went on to study the role it might play in the cell. For this purpose, M_2tail(368-466) fused to the fluorescent protein EGFP in pcDNA3, that is under the control of a strong CMV promoter, was expressed in HEK293 cells in order to study the subcellular localization of this domain. Confocal microscopy demonstrated a striking mitochondrial localization of the M_2tail(368-466)-EGFP construct (**Fig. 4a**). We confirmed this observation by co-staining HEK293 cells with a conventional mitochondrial stain (Mitotracker Deep Red) and by co-expressing M_2tail(368-466)-EGFP with Tom20-mCherry, a fluorescently labeled construct targeted to the outer mitochondrial membrane (**Fig. S7a**). The observed mitochondrial localization of the M_2tail(368-466)-EGFP appeared in stark contrast to the canonical cellular localization of the M_2 receptor, as shown in **Fig. 4b** where the M_2 muscarinic receptor was C-terminally labeled with the red fluorescent protein mRuby2. Interestingly, very little expression of M_2tail(368-466)-EGFP was observed on the plasma membrane, as we confirmed by fluorescence correlation spectroscopy (14) (**Figs S7b-d**). By contrast, when the M_2tail(368-466)-EGFP was co-expressed with M_2stop228, a modest localization could eventually be detected also on the cell membrane thanks to a

reduction in diffusion coefficient of M_2tail(368-466)-EGFP, suggesting a chaperon activity of the M_2 N-terminal domain (M_2trunk) (**Figs 7e-g**) and hence explaining the [^{3}H]NMS binding observed in cells transfected with either M_2stop228 or cotransfected with M_2trunk(1-228) and M_2tail(368-466) (**Table 1**). Likewise, constructs such as M_2tail(368-466)-mRuby2 (a red monomeric fluorescent protein) and M_2tail(368-466)-tdTomato (a tandem-dimer red fluorescent protein) also displayed clear mitochondrial localization (**Figs S7h-i**), ruling out bias due to the fluorophore used.

Localization of the M_2 C-terminal fragment generated by cap-independent expression under the control of the i3loop IRES

We then sought to express the C-terminal fragment of the M_2 receptor under the control of the i3loop IRES rather than a viral promoter, to further exclude the possibility that the observed localization of the M_2 carboxyl terminal fragment were due to overexpression of the construct. HEK293 cells were transfected with the construct M_2-mRuby2-STOP-M_2-i3-tail-EGFP which contains the full wild type M_2 receptor, mRuby2-labeled at the C-terminal, fused to the C-terminal part of the M_2 receptor starting at nucleotide 685 of the i3 loop, following the stop codon of mRuby2, and ending with a C-terminal EGFP sequence. Through this experimental strategy, the expression of M_2tail(368-466)-EGFP is regulated by the IRES, and the mechanism of C-terminal fragment production is therefore close to physiological. The expression of EGFP confirmed that the *in vivo* production of the M_2tail(368-466) is regulated by the IRES within the i3 loop. In addition, the processed receptor fragment was eventually observed to be predominantly confined to the cytosol and the mitochondrial network (**Fig. 4c**).

Notably, when the M_2-EGFP fusion protein was expressed and the cells were co-stained with Mitotracker, a faint EGFP signal was also observed in the mitochondrial regions (**Fig. S8a**), although the expression of the full-length receptor masks this effect and makes quantification difficult. On the other hand, **Fig. 4d** shows that, when the M_2fr.sh-EGFP mutant was expressed in HEK293 cells, the IRES generated C-terminal fragment of the M_2 receptor still localized to the mitochondria. As mentioned above, in this construct the masking effect of the EGFP fused to the full-length receptor is removed (see also **Fig. S1**). Similar mitochondrial localization was also observed when we transfected HEK293 cells with M_2fr.sh-mRuby2 (**Fig.**

S8b), ruling out possible effects due to the specific fluorophore used as a tag. We obtained comparable findings also in COS-7 cells (**Fig. S8c**).

Mitochondrial import of the C-terminal fragment of the M_2 receptor was further verified by immunoblotting of protein extracts from purified mitochondria of HEK293 cells transfected with myc-tagged M_2 receptor, M_2tail(368-466) and M_2M368A. **Fig. 4e** shows that in purified mitochondria (unlike in the cytosolic and microsomal supernatants originating from the purification process, **Fig. S8d**), only the protein bands associated to the M_2 C-terminal fragment were visible.

Notably, no mitochondrial import was visible for the M_2M368A, confirming that the third in frame methionine (M368) in the i3 loop of the M_2 receptor is necessary for the C-terminal fragment production and its localization in the mitochondria.

A consistent result was observed when mitochondria were purified from the heart and spleen of the Chrm2/tdtomato mice **Fig. 4f** (the cytosolic fraction is shown in **Fig. S8e**). A band at ~75 kDa, matching the molecular weight of the M_2 C-terminal domain, was clearly visible. We conclusively confirmed that this is the fingerprint associated to the M_2 C-terminal fragment, by purifying mitochondria from HEK293 cells expressing the construct M_2tail(368-466)-tdtomato. **Fig. 4g** (cytosolic fraction is shown in **Fig. S8e**) shows a ~75 kDa protein band matching closely the bands observed in mitochondria from mice tissues, in addition to lower molecular weight bands most likely arising from degradation of the tdtomato tag.

Mitochondrial localization of the M_2tail originating from the wild type M_2 receptor was finally confirmed by relative abundance estimates of EGFP and M_2 receptor from parallel reaction monitoring (PRM)-based mass spectrometry measurements **Fig. S9**. Samples were prepared by generating mitochondrial and cytosolic fractions (**Methods**) from HEK293 cells, expressing M_2-EGFP and a set of control constructs, including M_2tail(368-466)-EGFP, pmito-EGFP (an EGFP fused to the mitochondrial leading sequence of the cytochrome c oxidase subunit 8A (COX8A)), lifeact-EGFP (a cytosolic protein) and Epidermal Growth Factor receptor fused to EGFP (EGF-EGFP). A 15-aminoacid long peptide originating from EGFP was screened. The bands intensities of the cytosolic fraction, were normalized to consider both the overall loading variability as well as the relative transfection efficiencies among the samples. Notably, we observed a mitochondrial enrichment of the EGFP derived peptide as well the receptor-specific peptide originating from the M_2 receptor, in agreement with the positive mitochondrial localization control.

Mechanism of import of the M_2 carboxyl terminal fragment into the mitochondria and localization within the organelle

To gain further insight into the dynamics of the M_2 C-terminal fragment import within the mitochondria, we first monitored the kinetics of colocalization between mitochondria and EGFP in cells transfected with M_2tail(368-466)-EGFP. In cells observed for several hours, starting at 5h after transfection (**Fig. 4h**), the construct was found initially expressed in the perinuclear region, likely the endoplasmic reticulum, indicating that at least the initial step of subcellular trafficking of the M_2tail(368-466)-EGFP is the same as for the full length receptor (15). At this time (5h post-transfection), almost no colocalization with the Mitotracker-stained mitochondria was visible. However, at 6h post-transfection, the colocalization level increased significantly, and the M_2 C-terminal fragment was either found in the cytosol or in the mitochondria. At 9h post-transfection the colocalization at the mitochondria was well visible. We quantified the colocalization level over time using the Manders' coefficients (See **Methods**). The resulting chart, indicates that almost half of the mitochondrial import occurred within 6h post-transfection.

This value is qualitatively in agreement with what we observed using an in-vitro assay to determine the import of the M_2 carboxyl terminal into isolated mitochondria (see Methods). To this end, we used mitochondria form *S. cerevisiae*, which is a robust and well-studied system for protein import assays. **Fig. S10a** shows the autoradiography experiment of isolated, intact, mitochondria incubated with 35S-labelled full length muscarinic M_2 receptor or M_2tail(368-466), made using a reticulocyte in vitro translation system. The data show that the full-length receptor was not imported into mitochondria. On the other hand, the M_2tail(368-466) displays a clear mitochondrial import already after 5 minutes and increasing over time, up to 30 minutes. Interestingly, this import (**Fig. S10b**) appears to be independent upon the transporters of the outer membrane Tom5, Tom6, Tom7 and Tom70, whereas the import of an inner membrane protein, the ADP/ATP carrier (AAC), used here as a control, depends on Tom70. Upon extraction with carbonate most of M_2tail(368-466) was found in the pellet, and therefore presumably integrated in a membrane. Furthermore Blue native analysis suggests that the mitochondrially imported M_2tail(368-466) is not a monomer but rather it is part of a larger complex of approximately 180 kDa **Fig. S10c**.

All together these data indicate that the import of the M_2tail(368-466) leads to its localization in one of the mitochondrial membranes, to form a complex with other native mitochondrial proteins.

To further discriminate if the construct is on the outer or inner mitochondrial membrane, we set up a fluorescence assay based upon GFP fluorescence complementation (16). HEK293 cells were first transfected with two constructs: M_2tail(368-466)-GFP11, in which a short 16 amino acids peptide of GFP was fused at the C-terminus of M_2tail(368-466), and mito-GFP1-10, in which the COX8A was N-terminally fused to the other GFP fragment containing the remaining 10 beta strands (See **Methods**). **Figure S10d** shows the successful recombination of the two within the mitochondrial matrix. We then applied this approach to the full length M_2 receptor, by generating the M_2-GFP11 construct and by transfecting it in HEK293 cells. **Fig. 4i** shows a green signal from the recombined GFP visible in the mitochondria. All together these data suggest that the M_2 C-terminal fragment is localized in the inner mitochondrial membrane, with its own C-terminal domain facing the matrix.

This interpretation appears to be confirmed in cells expressing the M_2stop228-myc receptor and examined by electron microscopy (**Fig. S10e**) after immune-gold labelling. As shown in **Figs S10f-g**, gold particles were observed only in mitochondria, and at this stage they appeared localized either to the mitochondrial matrix or to the lumen of the cristae (**Figs S10h-k**).

Functional role of the C-terminal fragment in the mitochondria

The next step of our investigation concerned the obvious question about the functional effects, if any, that the observed localization of the M_2 C-terminal fragment might have on the mitochondrial activity, and -more generally- on the energy metabolism of the cell. To investigate this aspect, we measured the extent of oxygen consumption in COS-7 cells expressing M_2-EGFP, M_2tail(368-466)-EGFP or the sole EGFP as a control. Initially, we normalized the expression of the three proteins to the amount of EGFP expressed in the cells, then the metabolic functions were assayed on a Seahorse instrument using cells transfected with normalized amounts of plasmids (**Fig. 5a**).

Our data did not show a significant difference in total oxygen consumption capacity between cells transfected with cytosolic EGFP and the untransfected control. However, a significant decrease of oxygen consumption was found in cells transfected with M_2-EGFP and even more so with M_2tail(368-466)-EGFP (**Fig. 5a**).

Notably, the basal oxygen consumption rate (OCR), in starvation-stress conditions, was profoundly decreased in M_2tail(368-466) cells and to a smaller extent in M_2 cells compared to EGFP and empty control cells (see also the time-course in **Fig. S11a**). These results are in line with what was observed using a Clarke-type oxygen electrode (**Supplementary Materials and Figs S11b-c**).

A cell apoptosis assay, based on the detection of activated caspase-3 (17), did not show substantial differences among the tested mutants (**Fig. S11d**). The overexposed western blot showed a tiny amount of activated caspase-3 in most of the transfected COS-7 cells, indicating that the expression of M_2tail(368-466) in mitochondria, in agreement with the qualitative post-starvation data shown in **Figs S11e**, does not induce fragmentation of the mitochondrial network and cell apoptosis.

To test whether the C-terminal-M_2 fragment effects on mitochondrial oxygen consumption could alter the production of Reactive Oxygen Species (ROS), the measurements were combined in a single cell assay. Remarkably, ROS production (assayed using a fluorescence readout kit, where the fluorochrome becomes activated in contact with oxidized species) was clearly reduced within and in proximity of mitochondria of cells expressing a high level of the M_2tail(368-466) (**Fig. 5b**). By regrouping individual mitochondria in classes according to the level of the ROS marker expression, an actual inverse correlation between the amount of receptor fragment (Green Fluorescence) and the production of ROS (Red Fluorescence) was revealed.

Cell growth was also found to be affected depending on which of the constructs was transfected. Notably, transfection of HEK293 cells with the wild type M_2 receptor reduced significantly cell growth compared to the control, whereas cells transfected with the mutant M_2M368A, that do not express the M_2 C-terminal fragment (**Fig. 5c**), displayed a significantly higher growth. All cells were incubated with saturating concentration of the M_2 antagonist atropine throughout, in order to exclude effects on cell growth and proliferation due to the canonical receptor signaling.

These functional data are further supported by Fluorescence Resonance Energy Transfer (FRET) data aimed at investigating the molecular interactions of the mTurquoise2 labeled M_2tail(368-466) with mitochondrial proteins. Based on the oxygen consumption data (**Fig. 5a** and **Fig. S11a**) we chose as primary target the F_0F_1 ATP Synthetase complex, also indicated as complex V (CV), where the γ subunit was labeled with mCitrine, a fluorescent acceptor. The γ subunit is located towards the mitochondrial matrix. We further monitored

interactions with an intermembrane space protein (SMAC) and a protein localized to the mitochondrial matrix (COX8a), both fused to the mCitrine fluorescent acceptor. As clearly illustrated in **Fig. 5d**, FRET efficiency, an indicator of molecular interaction, is significantly larger for M_2tail(368-466)-CV pair than both the intermembrane space SMAC and the matrix COX8a. The latter result is particularly relevant, as it indicates that the interaction is specific, and not simply due to molecular proximity of the overexpressed constructs within the mitochondrial matrix.

Cell stress upregulates M_2 C-terminal expression and mitochondrial localization

Having established that the C-terminal fragment localizes in the mitochondria and affects the cell oxygen consumption rate, we looked at the effect of stress on the level of expression of the C-terminal fragment. Stressed cells attenuate their translational activity via phosphorylation of the initiation factor eIF2α. However, certain mRNAs may be insensitive to eIF2α phosphorylation level if their translation is regulated by IRES. Under these conditions their expression is bound to increase rather than to attenuate (18,19).

Therefore, we transfected COS-7 cells with the Sirius-M_2i3(417n)-EGFP reporter construct and stressed by starvation for three hours by replacing the culture medium with HBSS or PBS. During this time interval, the green fluorescence was seen to gradually increase up to 1.4 times the basal level observed in HBSS-starved cells and 3.5 times for PBS-starved cells (**Fig. 5e**), confirming that the C-terminal fragment expression is upregulated in response to stress conditions such as cell starvation. The same experiment was reproduced in single cells, displaying an increase of the average EGFP/Sirius ratio upon HBSS starvation in HEK293 cells (**Fig. S11g**).

We further used the GFP fluorescence complementation assay to emphasize the importance of stress in the pattern of expression of the M_2 gene. HEK293 cells were co-transfected with M_2-GFP11 and Mito-GFP1-10. HEK293 cells grown in culture medium predominantly expressed the full M_2 receptor protein (**Fig. 5f**). The green fluorescence detected in the plasma membrane is explained with the chaperoning effect of M_2-GFP11 on Mito-GFP1-10 before its sorting to the mitochondria. In sharp contrast, when HEK293 cells were first transfected with Mito-GFP1-10 and, 24h later, transfected with M_2-GFP11 followed by a 6 h starvation in HBSS, the pattern of expression changed drastically: IRES mediated translation of the M_2tail(368-466) fragment led to a predominantly mitochondrial green fluorescence signal of the complemented GFP (**Fig.**

5f). These results are in line with our observation that the IRES mediated C-terminal fragment localization to the mitochondria in cells expressing the construct *M_2-mRuby2-STOP-M_2-i3-tail-EGFP* was enhanced upon cell starvation, and drastically reduced upon mutation of the M368 (**Figure S12** and **Supplementary Materials**).

This observation was also supported by the lack of complementation of M_2tail-GFP11 with GFP1-10 when this last fragment was N-terminally fused to the targeting sequence of SMAC, a protein expressed in the mitochondrial intermembrane space (20) (**Fig. S13c**).

Mutation of the M368A via CRISPR/Cas9 affects cell growth and oxygen consumption rates in hiPSCs

We finally asked the question of what would be the effect of abolishing the translocation of the M_2 C-terminal fragment to the mitochondria, in a physiological and entirely label-free setting. To reach this goal we genetically engineered (see Methods) human induced pluripotent stem cell (hiPSC), to incorporate in both alleles of the M_2 gene the M368A mutation, that, based on our data, should be sufficient to significantly impair the M_2 C-terminal production and mitochondrial translocation. Wild type (wt) and M368A hiPSCs were cultured in pluripotency maintaining medium, and subsequently undirectedly differentiated upon exposure for seven days to DMEM-F12 medium, as described in the Methods. **Fig. 6a** shows confocal micrographs for wild type and M368A hiPSCs cultured in E8 medium respectively, with the M368A hiPSCs displaying a mildly more spread-out phenotype. We shall note here that the M_2 receptor has been found to be expressed in PSCs lines, and it has been shown to play a role in stem cell differentiation (21,22). In this context, however, we were not interested in the canonical signaling of the receptor, and all experiments were performed with a saturating concentration of atropine, to block any activity of the receptor. We then evaluated cell proliferation, observing a significant increase in the proliferation of the M368A clone 72h after seeding **Fig. 6b**. The observation of an increased proliferation of the cells harboring the mutation that impairs the production and localization of the C-terminal fragment in the mitochondria, suggests that the same effect is at play here, as observed in the overexpression system (**Fig. 5a,b,c**). These results are supported by extracellular oxygen consumption assays performed, for both hiPSCs and differentiated hiPSCs (**Fig. 6c**). Our data suggest that the M368A cells indeed display an accelerated oxygen consumption rate, and that this effect increases as the cell progressively differentiates.

For comparison, the assay was also carried on HEK293 overexpressing the wild type M_2 receptor and the mutant M_2M368A (**Fig. S11f**). We could observe with this assay a reduced oxygen consumption of the wild type M_2 receptor compared to untransfected cells, in line with what was observed in **Fig. 5a**, and an increased oxygen consumption of the M_2M368A expressing cells, in line with what observed for the hiPSCs.

Discussion

Over the last 10 years, growing evidence has accumulated indicating that GPCRs can be functional and signal also at cellular locations other than the plasma membrane. These locations can be associated to their canonical trafficking pathways (such as sorting vesicles and endosomes) (23), but also to non-canonical locations, such as the nucleus, the nuclear membrane, the Golgi apparatus and the mitochondria (reviewed in Jong et al. BPJ 2018 (24)). Some of these locations are surprising, since many ligands are non-membrane permeable, and it is still debated how they can reach their target receptors at such intracellular locations.

Interestingly, the specific localization of these receptors appears to go hand in hand with a specific function. In these cases, activation/inhibition of mitochondrially localized GPCRs have been shown to specifically affect the organelle function, ranging from oxygen consumption rates to Ca^{2+} handling and even to apoptosis. Notably Benárd et al (25) showed that the CB_1R on the outer mitochondrial membranes affects neuronal energy metabolism; Suofu et al. (10) demonstrated that activation of the MT_1R by a mitochondrial melatonin pool can affect cytochrome C release. This is particularly interesting, since cytosolic cAMP does not appear to be able to activate mitochondrial PKA, and hence a mitochondrially localized GPCR signalosome appears to be required to enable such downstream signaling cascade (26).

However, other non-canonical mechanisms are also possible for the regulation of mitochondrial function. It is well known that GPCRs are subject to interindividual variability, arising, for example, from mRNA alternative splicing (i.e. the process which allows the recombination of exons) which leads to different isoforms which may present distinct signaling and localization properties (27). Receptor variants with different functional and localization properties may also occur due to other processes. For example, our comprehension of eukaryotic translational regulation is facing a rapid expansion, as exemplified by the

observation that small open reading frames (smORFs), also within lncRNAs, are an important class of genes, oftentimes with mitochondrial localization (28).

In this study, for the first time, we provide evidence that an IRES sequence drives expression of a membrane receptor fragment and acts as a regulator of its expression levels and function. IRES sequences are distinct regions of the mRNAs that are capable of recruiting ribosomes in the proximity of an internal initiation codon and translate transcripts in a cap-independent manner (5,6,29-31). Here, we show that an IRES sequence is located within the third intracellular loop of the M_2 muscarinic receptor, where it plays a crucial role in regulating the expression of its carboxy-terminal domain, which we identified as M_2tail(368-466).

We assessed the IRES-driven expression of the C-terminal fragment through a broad set of constructs, meant to exclude alternative synthesis mechanisms such as stop-codon read-through, and a diversified palette of techniques. Radioligand binding data (**Table 1**) pointed to the necessity of the C-terminal fragment synthesis, in order to explain the observed downstream signaling in mutants carrying a stop codon in the initial portion of the i3loop of the M_2 receptor, upstream of M368. Fluorescence microscopy allowed us visualizing the production of the EGFP-tagged C-terminal fragment in these receptor mutants (**Fig. 1d**). We further detected its production by Western blotting on protein extracts from cells; here the C-terminal fragment gives rise to two bands: the lower of the two (~15 kDa) matching the expected molecular weight of the M_2tail based on the aminoacid sequence. On the other hand the ~22 kDa band intensity is likely the result of postranslational processing of the M_2tail((368-466) fragment: the ~8kDa shift may point to mechanisms such as glycosylation, ubiquitylation, SUMOylation or even non-canonical Ubiquitinylation (Davies et al. Nat. Comm. 2021). Such mechanisms need to be further identified and will be the focus of a follow-up work.

We further performed Western blotting from heart and brain tissues from knock-in mice carrying a C-terminally tagged M_2 receptor (tdtomato) and under the control of the endogenous promoter/enhancer sequences (**Fig. 2a-c**).

Mutagenesis of key residues within the i3 loop of the M_2 receptor allowed us to pinpoint the 3rd in-frame methionine as the most likely candidate for the beginning of the cap-independent translation (**Fig. 3**). This observation appears to be supported by the observation of a peak in ribosome coverage around the M368 seen in ribosome profiling databases (as reviewed in Ingolia et al.(32)), and particularly prominent in those from left ventricle cardiomyocytes, where M_2 receptor expression is known to be abundant (28).

To our surprise, in contrast to the plasma membrane localization of the wild type, full length M_2 receptor, the C-terminal fragment was localized mostly in mitochondria. This localization occurred markedly when overexpressing the C-terminal fragment M_2tail(368-466), but could be also clearly detected when the C-terminal fragment was expressed under the control of the IRES sequence of the full-length receptor (**Fig. 4 c,d**).

We devised several strategies to detect the localization of the IRES-driven fragment in the mitochondria by avoiding the cell-wide background signal from the full-length receptor. **Fig. 4c,d** show two prominent examples, namely relying on spectrally unmixing the two components, or by sending out of frame the EGFP at the C-terminus of the full-length receptor. By studying mitochondria purified from HEK293 cells we could confirm that the mutation of the M368, which we identified as the starting point of the IRES-mediated translation, is sufficient to suppress any mitochondrial targeting of the M_2 C-terminal fragment, and most likely, its synthesis altogether (**Fig. 4e**).

We then addressed the mechanism of mitochondrial import of the C-terminal fragment and its localization within the organelle. Our data, originating both from live cell import kinetics (**Fig.4h**) as well as from in-vitro import into isolated mitochondria (**Fig. S10**), support the notion that the fragment becomes rapidly imported into mitochondria following translation in the cytosol. Once inside the mitochondria, it undergoes processing leading to the appearance of a lower molecular weight band, observed both in Western blots from whole cell and mice tissue protein extracts, as well as from purified mitochondria. The fragment is found predominantly in a carbonate-insoluble fraction, i.e. a membrane, and it appears to form a high molecular weight complex of ~180 kDa with other mitochondrial proteins (**Fig. S10c**).

Fluorescence complementation assays (**Fig. 4i**) and electron microscopy (**Fig. S10d**) suggest that the M_2 C-terminal fragment predominantly resides in the inner mitochondrial membrane, with its own C-terminal domain exposed towards the matrix. Future work should clarify the precise import pathway.

Most importantly, our data show that mitochondrial oxygen consumption was reduced by the M_2tail(368-466) (**Fig. 5a,b**), and also cell proliferation was affected (**Fig. 5c**). Under integrated stress response, namely aminoacid starvation, IRES-mediated production of the C-terminal fragment was increased (**Fig. 5d-f**). On these bases, the M_2tail might be needed in mitochondria as a means to reduce mitochondrial basal oxygen consumption and ATP-linked respiration. An important consequence of reduced respiration is the lower level of ROS produced in mitochondria, as we observed in agreement with this hypothesis.
This observation was confirmed in physiological, label-free conditions, by genetically editing human induced pluripotent stem cells in order to suppress the synthesis of the M_2 C-terminal fragment mutating the starting methionine M368. Increase of cell proliferation of this clone compared to its wild type counterpart, together with an increase of oxygen consumption rates (**Fig. 6**), corroborates our hypothesis that the M_2 C-terminal fragment reduces oxygen consumption upon reaching the mitochondria. The effect was further amplified when the cells were undirectedly differentiated, and it was consistent with the shift of the cell phenotype towards oxidative phosphorylation (33).

The mechanism by which the M_2tail(368-466) may reduce oxygen consumption in mitochondria and its meaning needs to be further explored. Our FRET data (**Fig. 5d**) indicate that the M_2 C-terminal fragment has a specific interaction with the F_0F_1 ATP-synthase complex, supporting the concept that it inhibits the activity of this enzyme, thus leading to the observed reduction in oxygen consumption rates. Future work should clarify the precise import pathway and the inhibitory effect of M_2tail(368-466) on F_0F_1 ATP-synthase. Nonetheless, since ROS production is implicated in the pathogenesis of several diseases (34), we would propose the hypothesis that increased localization of the M_2 C-terminal fragment in mitochondria, as it occurs under integrated stress response, might have protective effects (**Fig. 7**).

In broader terms, protection of mitochondria by unconventional import mechanisms to allow localization within the organelle of specific proteins has been previously observed for cells that undergo stress conditions (35). The mechanism of IRES-dependent modulation of translation and consequent mitochondrial targeting of the translation product of a GPCR may provide another means, completely unrelated to the canonical signaling function of this class of membrane receptors, of a generic cellular response to overcome different types of stress by modulating the mitochondrial proteome and adjusting the mitochondrial bioenergetic state.

Materials and Methods

Experimental Design

The Materials and Methods section should provide sufficient information to allow replication of the results. Begin with a section titled Experimental Design describing the objectives and design of the study as well as prespecified components.

Generation of mutant muscarinic M_2 receptors

Multiple receptor mutants were constructed starting from the human M_2 muscarinic receptor expressed in the pcD vector (36). The constructs are sketched in **Fig. S1**. The two expression plasmids referred as M_2trunk(1-283) (containing transmembrane domains I-V and the N-terminal portion of the third cytoplasmic loop) and M_2tail(281-466) (containing transmembrane domains VI and VII, and the C-terminal portion of the third cytoplasmic loop) were described previously (12).

M_2stop228 – This plasmid was created by substituting codon 228 (CAA) with a stop codon (TAA) at the N-terminal of the i3 loop of the wild type M_2 receptor.

M_2stop228/stop400 – This plasmid was created by inserting an additional stop codon – TGG was substituted with TAA – at the position codon 400 of the TM region VI of the M_2stop228 mutant.

M_2stop400 – This plasmid was created by substituting codon 400 (TGG) with a stop codon (TAA) in the TM region VI of the wild type M_2 receptor.

M_2stop196 – This plasmid was created by substituting codon 196 (TAT) with a stop codon (TAA) in the TM region V of the wild type M_2 receptor.

M_2stop196/stop400 – This plasmid was created by inserting an additional stop codon in the TM region VI of the M_2stop196 mutant, where TGG was substituted with TAA at position of the codon 400.

M_2stop228/fr.sh. – This plasmid was created by inserting four bases (AATT) fifteen nucleotides downstream of the stop codon to create a shift in the correct reading frame of the M_2stop228 mutant.

M_2stop228/hairpin – This construct was created by inserting a 42 bases long sequence (AGGGGCGCGTGGTGGCGGCTGCAGCCGCCACCACGCGCCCC), fifteen nucleotides downstream of the stop codon of the M_2stop228 mutant. Upon transcription, this palindromic sequence has been shown to form a hairpin structure with a ΔG value of −64 kcal/mol that blocks effectively ribosome scanning (37,38).

M_2stop228/stop248, M_2stop228/stop296 and M_2stop228/stop368 – These three constructs were obtained by substituting the three in-frame ATG codons (1. ATG 248, 2. ATG 296 and 3. ATG 368) with the stop codon TAA downstream of the stop228 of the M_2stop228 mutant.

M_2trunk(1-228) – This plasmid was created by substituting codon 228 (CAA) with a stop codon (TAA) at the N-terminal of the i3 loop of the wild type M_2 receptor followed by removal of the downstream sequence.

M_2tail(368-466) – This construct was created by removing all bases of the M_2 receptor sequence up to codon 368 (ATG) of the C-terminal of the i3 loop. The resulting plasmid encodes for a polypeptide fragment that contains the trans-membrane domains VI and VII along with the C-terminal portion of the third cytoplasmic loop.

M2(M368A) – In this construct the third in-frame methionine of the i3-loop of the M_2 muscarinic receptor (ATG) was mutated to alanine (GCG).

M_2-Myc, M_2stop228-Myc, M_2stopM368A-Myc, M_2tail(368-466)-Myc and M_2stop40-Myc – M_2-Myc was purchased from OriGene. This plasmid encodes the human M_2 receptor with a

Myc (tag at the C-terminus of the protein. M_2stop228-Myc was obtained by replacing the 0.9 Kb BmtI-PspOMI fragment of the M_2stop228 mutant with the corresponding fragment of M_2-Myc. M_2stop400-Myc was obtained by substituting the codon 400 (TGG) with a stop codon (TAA) of the M_2-Myc. All the constructs have an additional DDK tag after the C-Myc. Subsequently, all C-Myc constructs were extracted by PCR and subcloned into a bicistrionic pVitro2-MCS plasmid (Invivogen), allowing for the expression of a reporter gene (in our case the red fluorescent protein mRuby2) after an IRES sequence, in order to check for transfection efficiency.

Generation of bicistronic constructs expressing Sirius and EGFP proteins (Fig. 3a)

Sirius[PacI-M_2i3(685-1101)]EGFP – This bicistronic construct was created by inserting the i3 loop of the muscarinic M_2 receptor, from nucleotide 685 to nucleotide 1101, between the ultramarine fluorescent protein (Sirius) and the green fluorescent protein (EGFP). Eight nucleotides corresponding to the recognition site of the PacI enzyme were inserted between Sirius and the i3 loop of the wild type M_2 receptor to alter the reading frame downstream of the Sirius stop codon. Hereafter this plasmid is referred to as Sirius-M_2i3(417n)-EGFP.

Sirius[PacI-M_2i3(685-699)-Hairpin-G]EGFP – This bicistronic construct was created by inserting a 42 nucleotides hairpin loop (see above) between Sirius and the EGFP fluorescent protein. The hairpin loop was spaced from the Sirius stop codon by inserting a PacI recognition sequence and 15 nucleotides of the M_2 i3 loop sequence comprised between nucleotide 685 and nucleotide 699. A G nucleotide was also inserted following the 42 nucleotides of the hairpin loop and upstream of the initial ATG triplet of the EGFP to restore a correct reading frame. Throughout the text we referred to this plasmid as Sirius-H-EGFP.

Sirius[PacI-M_2i3(685-699)-Hairpin-G-PacI-M_2i3(685-1101)]EGFP – This bicistronic construct was created by adding 417 nucleotides of the i3 loop of M_2 from nucleotide 685 to nucleotide 1101 to the plasmid *Sirius[PacI-M_2i3(685-699)-Hairpin-G]EGFP*. An

additional PacI restriction site was also inserted upstream of this segment of the i3 loop. Throughout the text we referred to this plasmid as Sirius-H-M_2i3(417n)-EGFP.

Sirius[PacI-M_2i3(685-699)-Hairpin-G-PacI-M_2i3(685-699/1072-1101)]EGFP – This bicistronic construct was created by deleting from the plasmid *Sirius[PacI-M_2i3(685-699)-Hirpin-G-PacI-M_2i3(685-1101)]EGFP* 372 nucleotides of the M_2 i3 loop, from nucleotide 700 to nucleotide 1071. Throughout the text we referred to this plasmid as Sirius-H-M_2i3(15n/30n)-EGFP.

Sirius[PacI-M_2i3(685-699)-Hirpin-G-PacI-M_2i3(685-699)]EGFP – This bicistronic construct was created by adding 15 nucleotides of the i3 loop of M_2 from nucleotide 685 to nucleotide 699 to the plasmid *Sirius[PacI-M_2i3(685-699)-Hirpin-G]EGFP*. An additional PacI restriction site was also inserted upstream of this short segment of the i3 loop. Throughout the text we will refer to this plasmid as Sirius-H-M_2i3(15n)-EGFP.

Sirius[PacI-M_2i3(685-699)-Hirpin-G-PacI-M_2i3(685-1071)]EGFP – This bicistronic construct was created by adding 387 nucleotides of the i3 loop of M_2 form nucleotide 685 to nucleotide 1071 to the plasmid *Sirius[PacI-M_2i3(685-699)-Hirpin-G]EGFP*. An additional PacI restriction site was also inserted upstream this long segment of the i3 loop. Throughout the text we will refer to this plasmid as Sirius-H-M_2i3(387n)-EGFP.

Mutants of the Sirius-H-M_2i3(15n/30n)-EGFP plasmid – Based on the sequence alignment of amine and adenosine GPCRs, several conserved nucleotides were mutated in order to define the putative IRES sequence. These mutants are reported in **Fig. 3b**.

The fluorescence intensities of the two spectral bands were quantified by the use of a fluorometer and the EGFP intensity values normalized to those of Sirius.

Constructs for fluorescence microscopy

M_2-EGFP – The wild type M_2 muscarinic receptor was cloned into the pEGFP-N1 expression cassette, between the restriction sites HindIII and XbaI.

M_2-mRuby2 – The wild type M_2 muscarinic receptor was cloned into the mRuby2 vector (Addgene plasmid #40260).

M_2tail(368-466)-EGFP – The M_2tail(368-466)-EGFP was constructed so that the receptor protein would start from the third in-frame methionine of the M_2 i3 loop (M368). The EGFP gene was fused C-terminally following a short restriction site sequence (TCTAGA) of the XbaI enzyme.

M_2tail(368-466)-mRuby2 – The M_2tail(368-466)-mRuby2 was constructed so that the receptor protein would start from the third in-frame methionine of the M_2 i3 loop (M368). The mRuby2 gene was fused C-terminally following a short restriction site sequence (TCTAGA) of the XbaI enzyme.

M_2-mRuby2-STOP-M_2-i3-tail-EGFP – This mega construct was obtained by fusing two preceding constructs, M_2-mRuby2 and M_2tail(368-466)-EGFP, in a unique plasmid, but the M_2tail started at codon 229 (M_2tail(229-466)-EGFP). After the stop codon of mRuby2 and before the codon 229 of M_2tail was inserted a short restriction site sequence (TCCGGA) of the BspEI enzyme (**Fig. 4**).

M_2(M368A)-mRuby2-STOP-M_2-i3-tail-EGFP – This mega construct is analogous to *M_2-mRuby2-STOP-M_2-i3-tail-EGFP, but* the third in-frame methionine of the i3-loop of the M_2 muscarinic receptor was mutated to alanine (M368A) (**Fig. S1**).

M_2fr.sh-EGFP – A single base insertion (G) upstream of nucleotide 1102 of the wild type M2 receptor, just before the third in-frame methionine of the i3-loop (M368), induces a frame shift that, following 2 aminoacids, generates a stop codon (TAA) in the amino acid position 370 of the new reading frame. The construct is then fused to EGFP.

M_2fr.sh-mRuby2 – As above, but the EGFP is replaced by a mRuby2.

M_2-GFP11 – A short peptide 16 aminoacids long from the GFP protein, GFP11, was fused to the C-terminus of the muscarinic M_2 receptor. GFP11 was custom syntethised and inserted as a linker between the XbaI and XhoI restriction sites in the plasmid backbone of M_2-EGFP.

Mito-GFP1-10 – The mitochondrial targeting sequence of the cytochrome c oxidase subunit 8A (COX8A) was fused to the N-terminal of GFP1-10 fragment of GFP. GFP1-10 was purchased from Addgene as Addgene plasmid 70219.

Mito-GFP11 – The mitochondrial targeting sequence of COX8A was fused to GFP11 fragment. Mito sequence was obtained from Addgene plasmid 23348.

SMAC-GFP1-10 – The mitochondrial targeting sequence of the SMAC protein was fused to the N-terminal of GFP1-10 fragment. SMAC was obtained from Addgene plasmid 40881.

SMAC-GFP11 – The mitochondrial targeting sequence of the SMAC protein was fused to GFP11 fragment.

M_2tail(368-466)-GFP1-10 – The GFP1-10 fragment was fused to the C-terminus of the muscarinic M_2tail(368-466) receptor fragment.

M_2tail(368-466)-GFP11 – The GFP11 fragment was fused to the C-terminus of the muscarinic M_2tail(368-466) receptor fragment.

SMAC-mCitrine – mCitrine was fused to the C-terminus of the mitochondrial targeting sequence of SMAC using restriction enzymes: BamHI and NotI. SMAC sequence was obtained from Addgene plasmid 40881. mCitrine originates from plasmid FLAGmMOR-mCitirine, in pcDNA3.1.

Mito-mCitrine - mCitrine was fused to the C-terminus of the mitochondrial targeting sequence of COX8A using restriction enzymes: BamHI and NotI. Cox8A (Mito) sequence was obtained from Addgene plasmid 23348.

CV-mCitrine - mCitrine was fused to the C-terminus of the mitochondrial targeting sequence of Complex V (CV) using restriction enzymes: EcoRI and NotI. CV sequence was obtained from Addgene plasmid 213884.

M2tail-mTurquoise2 - mTurquoise2 was fused to the C-terminus of M2tail using the restriction enzymes: XbaI and NotI. mTuquoise2 originates from the plasmid pc-FLAG-mTq2-b2AR, in pcDNA3.1.

Constructs for in-vitro mitochondrial import assays

PSP64-M_2tail(368-466)-5Met - The vector backbone PSP64 (courtesy of Ruaridh Edwards). The following primers: FWD: ATGATGTAAtctagaggaggcggacgc, REV: CATCATCATccttgtagcgcctatgttcttataatg were used to add five methionines to the C-terminal domain of the M_2tail(368-466)-GFP11 template (see above) using Q5® Site-Directed Mutagenesis Kit (New England Biolabs® Inc.). The construct was then extracted with appropriate restriction enzymes (HindIII and XbaI) and ligated into the vector backbone PSP64 (courtesy of Ruaridh Edwards).

PSP64-M2R-5Met – The following primers: FWD: ATGATGTAAtctagaggaggcggacgc REV: CATCATCATccttgtagcgcctatgttcttataatg were used to add five methionines to the C-terminal domain of to the M_2-GFP11 template (see above) using Q5® Site-Directed Mutagenesis Kit (New England Biolabs® Inc.). The construct was then extracted with appropriate restriction enzymes (HindIII and XbaI) and ligated into the vector backbone PSP64.

All constructs were sequenced either with a Genetic Analyzer 3500 (Applied Biosystem®) or by a professional sequencing service (LGC Genomics, Berlin).

Reverse transcription

Reverse transcription was performed using a 24-nucleotide antisense oligo (TTACCTTGTAGCGCCTATGTTCTT) directed against the last 24 nucleotides at the 3' end of the M_2 open reading frame. cDNA amplification was carried out with the same antisense oligo used for reverse transcription, together with a 24 nucleotides sense oligo (ATGAATAACTCAACAAACTCCTCT) directed against the first 24 nucleotides at the 5' end of the M_2 open reading frame.

Cell culture and transfection

COS-7 (African green monkey kidney fibroblast-like SV40 transformed cell line) and CHO (Chinese Hamster Ovary) cells (from American Type Culture Collection) were grown at 5% CO_2 and 37 °C, in high glucose Dulbecco's modified Eagle's medium (DMEM) supplemented with 10% fetal bovine serum (FBS), 2 mM L-glutamine, 50 IU/ml penicillin, and 50 mg/ml streptomycin, and non-essential amino acids. HeLa cells (from American Type Culture Collection) were cultured in the same medium, but with the double amount of L-glutamine. SHSY-5Y cells were cultured in Roswell Park Memorial Institute (RPMI) medium supplemented with 10% FBS, 2 mM L-glutamine, 50 IU/ml penicillin, and 50 mg/ml streptomycin. Media and reagents used for cell cultures were from Euroclone, PAN Biotech, Biochrome and Sigma-Aldrich. Cell transfection was performed using FuGene® transfection reagents (Promega) as recommended by the manufacturer. Eighty percent confluent cells were washed twice with free-serum medium and the mix of FuGene and plasmid DNA was added. In every experimental condition 6-8 µg of plasmid DNA per Petri (10 cm^2) were used. Cells were grown for 48 h post-transfection before use. In co-transfection experiments, half amount of each plasmid DNA was used. All microscopy experiments were performed with transiently transfected HEK293 (Human Embryonic Kidney, ECACC 96121229 from Sigma-Aldrich Chemie GmbH) and COS-7 cells. HEK293 cells were cultured in DMEM (Dulbecco's modified Eagle's medium PAN biotech, Aidenbach, Germany), supplemented with 4.5 g/L Glucose, 2 mM L-Glutamine, 10% FCS, 100 units/mL penicillin and 0.1 mg/mL streptomycin and maintained at 37 °C and 5% CO_2. Cells cultured in 15-cm dishes were split at a 1:36 ratio into 6-well plates containing poly-D-lysine (PDL)-coated 24 mm glass coverslips. Cells were transfected using Effectene transfection reagent (QIAGEN) according to the manufacturer's instructions. Cells seeded on PDL-coated coverslips in 6-well plates were transfected 16 hours after seeding with 0.6 µg plasmid/well.

Fluorescence microscopy

Fluorescence microscopy experiments were performed either on a Leica SP5 (or SP8) Confocal Microscopes, using HyD photon counting detectors and an Argon/Ion laser (or white light laser) source for 488 nm/633 nm excitation and a solid-state diode laser (or white light laser) for 561 nm excitation. A solid-state diode laser was used for 405 nm excitation. A 40x 1.3 NA objective was used,

and the electronic zoom was set to achieve a pixel size of 50 nm. For visualization, mitochondria of transfected cells were labelled for 30 minutes at 37 C with 50nM MitoTracker® Deep Red FM (Invitrogen™, Thermo Scientific).

Ligand binding studies

Cells were lysed 48 h post-transfection with ice-cold 2 mM EDTA, 1 nM Na-HEPES (pH 7.4), scraped with a rubber policeman in the presence of ~4 ml rinsing medium, and homogenized with a Polytron homogenizer (ULTRA-TURRAX) in binding assay buffer (50 mM Tris-HCl, pH 7.4, 155 mM NaCl, 0.01 mg/ml bovine serum albumin). Radioligand bindings were carried out at 37 °C for 3 h in a final volume of 1 ml. Non-specific binding was determined in presence of 1 μM atropine. For competition binding assays, increasing concentrations of carbachol (from 0.01 μM up to 10 μM) were used in presence of 200 pM [^{3}H]N-Methylscopolamine ([^{3}H]NMS; 78.9 Ci/mmol; PerkinElmer).

The bound ligand was separated from the unbound ligand using glass-fiber filters (Whatmann, GF/B) with a Brandel Cell Harvester, and filters were counted with a scintillation β-counter. K_D values of [^{3}H]NMS were calculated in direct saturation experiments, whereas carbachol Inibitory Concentration $(IC)_{50}$ values were calculated in competition curves, against 400 pM [^{3}H]NMS, fitted to one binding models using the iterative, non-linear least-squares regression analysis of OriginPro 7.5 software (OriginLab Corporation).

Phosphatidylinositol Breakdown Assay

Transfected COS-7 cells were incubated with myo-[^{3}H]inositol (23 Ci/mmol; PerkinElmer) for 48 h. Immediately before the experiment the cells were washed twice with phosphate-buffered saline and incubated for 15 min in Eagle's medium containing 10 mM LiCl and 20 mM HEPES. The medium was then replaced by 0.25 ml of the same medium containing the experimental agents. After a 1-hour incubation at 25 °C the reaction was arrested by the addition of 0.75 ml of 7.5% (w/v) ice-cold trichloroacetic acid followed by a 30-min incubation on ice. The trichloroacetic acid was extracted with water-saturated diethyl ether (3 × 4 ml), and levels of IP_1 determined by anion exchange chromatography.

Adenyl Cyclase Assay

COS-7 cells were transfected with plasmid(s) containing the receptor of interest plus adenyl cyclase V. 24 h after transfection the cells were detached with trypsin and re-cultured in 24-well plates. Following an additional period of 24 h culture, they were assayed for adenyl cyclase activity. The assay was performed in triplicate**.** In brief, cells were incubated in 24-well plates for 2 h with 0.25 ml/well of fresh growth medium containing 5 µCi/ml [^{3}H]adenine (PerkinElmer). The medium was then replaced with 0.5 ml/well of DMEM containing 20 mM HEPES, pH 7.4, 0.1 mg of bovine serum albumin, and the phosphodiesterase inhibitors 1-methyl-3-isobutylxanthine (0.5 mM) and Ro-20–1724 (0.5 mM). AC activity was stimulated by the addition of 1 µM forskolin in the presence or absence of carbachol. After 10 min of incubation at +30 °C the medium was removed, and the reaction terminated by addition of perchloric acid containing 0.1 mM unlabeled cAMP followed by neutralization with KOH. The amount of [^{3}H]cAMP formed under these conditions was determined by a two-step column separation procedure (referenza?).

Immunoblot of muscarinic M_2 receptor mutants transfected in HEK293 cells

Cells were seeded in 10 cm plates and transfected after 24h according to manufacturer protocols (Effectene, Qiagen) using 2 µg of plasmid DNA. 48h after transfection cells were washed (2x) in ice cold PBS. 200 µL per plate of ice-cold lysis buffer were added. Lysis buffer was a RIPA buffer: 50 mM Tris-HCL pH 8, 150 mM NaCl, 1% TRITON, 0.5% sodium deoxycholate and 0.1% SDS. The following compounds were added to the buffer to a final 1x dilution: 100x Halt Protease Inhibitor Cocktail (Thermo Fisher), 100x 0.5 M EDTA and (10x) 10 mM PMSF. Cells were then scraped and the cell lysate transferred to pre-cooled 1.5 mL Eppendorf tubes. The tubes were placed in a Thermomixer at 4 °C, 300 rpm for 30 minutes. Then the Eppendorf tubes were centrifuged for 30 minutes at 14000 rpm at 4 °C. The supernatant was then transferred to new Eppendorf tubes. Protein concentration in the cell lysates was quantified by a BCA assay (Pierce BCA Protein Assay Kit, from Thermo Fisher) according to manufacturer instructions.

Cell lysates were loaded into 10% polyacrylamide gels. Cell lysates were loaded using Laemmli

Buffer 2x (Sigma Aldrich) in equal mass. As a reference marker we loaded 5 uL of PageRuler Prestained Protein Ladder (Thermo Fisher). Gels were mounted into a Mini Protean Tetra Cell kit (BioRad) using 1x SDS running buffer. Gels were ran using a constant voltage of 90V for approximately 15 minutes, and afterwards at 130V for 45 minutes. Gels were transferred to PVDF membranes. Wet transfer was achieved by using the Mini Trans Blot Module (BioRad) in Wet Transfer Buffer (25 mM Tris pH 8.3, 192 mM Glycine and 20% MetOH) at 350 mA for 90 minutes. The immunoblotted membranes were then blocked in 5% Milk in TBS-T for 1 hour at room temperature. The membrane was then incubated overnight at 4 °C with primary antibody solution using the following concentrations depending on the antibody used: 1:1000 anti **β**-actin (13E5) rabbit primary antibody (Cell Signaling), 1:1000 anti myc-Tag (9B11) mouse primary antibody (Cell Signaling). After overnight incubation, the membranes were washed 3x 10 minutes in TBS-T and incubated at RT for 1 h with a secondary antibody (1:10000 anti-mouse IgG/(anti rabbit) HRP-linked antibody from Cell Signaling).

After the incubation with the secondary antibody, the membrane was washed 3x 10 minutes in TBS-T. Detection was achieved by eliciting HRP luminescence by incubating the membrane with SuperSignal WestFemto solution (Thermo Fisher) according to the manufacturer's instructions, and imaging the membrane using a c600 Transilluminator from Azure Biosystems.

Animal Experiments

All animal experiments were carried out according to the German animal welfare act, considering the guidelines of the National Institute of Health and the 2010/63/EU Directive of the European Parliament on the protection of animals used for scientific purposes. The animals had free access to food and water and were kept in individually ventilated cages under a 12h:12h light/dark regime (light from 6:30 am to 6:30 pm), a constant 22±2°C temperature and 55±10% humidity.

The transgenic line B6.Cg-Chrm2tm1.1Hze/J, also known as Chrm2-tdT-D knock-in, was obtained from 'The Jackson Laboratory' (Stock No: 030330). They are heterozygous animals, designed to have expression of a Chrm2/tdTomato fusion protein directed by the endogenous M2 muscarinic acetylcholine receptor promoter/enhancer sequences.

Tissue preparation and immunoblot of endogenous M_2 receptor in Chrm2-tdT-D knock-in mice

Mouse tissues were weighed out and ice-cold lysis buffer was added to approx. 0.2-0.5mg tissue/ml buffer (10mM K2HPO4, 150mM NaCl, 5mM EDTA, 5mM EGTA, 1% Triton X-100, 0.2% Na-deoxycholate. Fresh protease inhibitors PMSF 0.5mM, Na3VO4 0.1mM, NaF 50mM, Jenny's mix (Soybean trypsin inhibitor 3.2µg/ml, Aprotinin 2µg/ml, Benzamidin 0.5mM) were added to the buffer. Samples were first homogenized, and then pellet debris were centrifuged at 4°C for 30 minutes at max speed (tabletop) and the supernatant (soluble proteins) was transferred into fresh tube (pellets = non-soluble proteins)

Protein concentration were determined with BCA assay. Cell lysates were loaded using Laemmli Buffer 2x (Sigma Aldrich) in equal mass (see above for the immunoblot procedure) into 8% polyacrylamide gels.

The membrane was then incubated overnight at 4 °C with primary antibody solution (1:1000 anti **β**-actin (13E5) rabbit primary antibody #4970 from Cell Signaling) (1:1000 anti GAPDH) (1:1000 anti-TdTomato rabbit primary antibody #632496 from Takara).

Isolation of mitochondrial fractions and immunodetection

Cells were seeded in 15 cm plates and transfected after 24h according to manufacturer protocols (Effectene, Qiagen) using 5 µg of plasmid DNA. 48h after transfection cells were harvested and centrifuged at 1000 rpm for 10 minutes, resuspended in NaCl 0.9% (w/v) and centrifuged at 1000 rpm for 10 minutes.

Mouse tissue were freshly excised and placed in ice cold PBS (1x) . The samples were washed with NaCl 0.9% (w/v). The homogenization steps were performed with Precellys Evolution Homogenizer, at 4500 rpm for 10 seconds.

The samples were processed according to manufacturer protocols (Qproteome Mitochondria Isolation Kit, Qiagen). From the different steps were obtained three different fractions: the cytosolic, the microsomal and the mitochondrial fraction.

The fresh mitochondrial pellet was resuspended in 150µL of ice-cold lysis buffer and the protein

concentration of the three fractions from each sample was quantified with a BCA assay (see above). Cell lysates were loaded into 12% polyacrylamide gels using an SDS loading buffer (6x solution: 2.28g Tris-HCl, 2.313 DTT, 6g SDS, 30% Glycerol and 0.03% bromophenol blue in a final volume of 50 mL) in equal mass (see above for the immunoblot procedure).

The membrane was then incubated overnight at 4 °C with primary antibody solution using the following concentrations: 1:1000 anti **β**-actin (13E5) rabbit primary antibody (#4970 from Cell Signaling), 1:1000 anti-tdtomato rabbit primary antibody (#632496 from Takara), 1:1000 anti **β**-tubulin mouse primary antibody, 1:1000 anti GAPDH mouse primary antibody, 1:1000 anti COXIV mouse primary antibody (#ab33985 from abcam).

Quantification of M_2tail(368-466) mitochondrial import kinetics from confocal time sequences

Before imaging, 2.5×10^4 HEK-TSA cells were seeded in each PDL-coated well of the μ-Slide 8 well (Ibidi) with DMEM (ScienCell™) supplemented with 10% FBS and 1% P/S overnight, and transfected with a total of 2 μg C-terminal EGFP tagged M_2 tail using Lipofectamine 2000 (Thermo Fisher Scientific) according to the manufacturer protocol after washing with 200 μL PBS and refreshing with 100 μL DMEM (ScienCell™) supplemented with 10% FBS and 1% P/S. After transfection for five hours, mitochondria of transfected cells were rapidly labelled with 50nM MitoTracker® Deep Red FM (Invitrogen™, Thermo Scientific) in FluoroBrite DMEM medium (Thermo Scientific) supplemented with 1% P/S for 20 minutes after the removal of old culture medium. After mitochondria labeling, the μ-Slide were washed twice with FluoroBrite DMEM medium (Thermo Scientific) and subsequently mounted onto the TCS SP8 confocal microscope (Leica) (See imaging). Firstly, the stage of the microscope was equilibrated in temperature, and the acquisition mode was set to the tile scanning. After storing the position of each desired transfected cells, the imaging mode was set to XYT and a HC PL APO CS2 40×/NA1.3 oil immersion objective was selected. Both DIC channel and HyD were utilized to obtain 512×512 pixels images. Laser wavelengths were set as described in the section Fluorescence Microscopy above. All settings remained the same throughout the whole measurement. Images were taken at every 30 minutes over a 5h interval. The images were afterwards analyzed by ImageJ software, using the Plugin 'JACoP'.

Briefly, the degree of colocalization between EGFP-tagged M_2tail(368-466) (CH1) and MitoTracker stained mitochondria (CH2) was quantified by Mander's colocalization coefficients (39). The two colocalization coefficients M1 ($M1 = \frac{CHB}{CH1}$) and M2 ($M2 = \frac{CHB}{CH2}$), CHB indicates overlapping pixels in channel 1 and channel 2. A threshold was determined for individual channel in order to distinguish specific signals from nonspecific ones. Due to their sensitivities to thresholds, the Pearson correlation coefficient (PCC)(40), as well as the faster decaying attribute of nonspecific signals, were also taken into account while estimating thresholds for each channel. For the analysis of each cell, the threshold for Mitotracker channel was kept constant. Whereas the threshold for EGFP channel was evaluated based on the PCC value.

Transfection and expression of split-GFP constructs in HEK293 cells

To perform the sequential split GFP complementation assay illustrated in **Figs 4h-i and 5f**, 3×10^5 HEK-TSA cells were seeded on a 10% poly-D-lysine (PDL)-coated 25mm coverslip in each well of a Falcon® 6-well flat-bottom plate (StemCell™) and cultured overnight. Cells were transfected using Effectene (see above) with a 0.4 µg Mito-GFP1-10 plasmid. The cells were then washed once with fresh 2 mL phosphate-buffered saline (PBS) first and supplemented with 1.5 mL fresh DMEM medium (ScienCell™) supplemented with 10% FBS and 1% P/S. After adding the transfection mixture, the cells were cultured overnight. After the first transfection, a second transfection of a 0.6 µg plasmid encoding either the C-terminal GFP11 tagged M_2tail(368-466) or M_2 receptor was performed using the Effectene Transfection Reagent (Qiagen). After washing each well with 2 mL PBS, the old medium was exchanged with 1.5 mL low glucose Minimum Essential Medium (MEM) (Gibco™, Thermo Scientific) supplemented with 1% P/S, in order to create a stress-like cell starvation condition. After a four hours starvation, the cells were fixed using 4% polyformaldehyde (PFA)/PBS at 37°C for 30 minutes and washed twice with PBS before imaging.

Oxygen consumption measured with the Seahorse assay

$5x10^4$ COS7 cells were seeded in seahorse 24MW plates with Complete media (DMEM supplemented with 10%FBS and 1X PS) and then incubated for about 4h at 37C in a cell incubator. After this incubation, cells were washed twice with Seahorse media supplemented with glutamate (1 mM), pyruvate (1 mM) and glucose (20 mM) and then incubated for 1h at 37 °C in an incubator without CO2 before being analyzed in the Seahorse XF Analyzers. In particular, the baseline cell oxygen consumption rate (OCR) was measured at the beginning of the assay, followed by measurements of ATP linked respiration and maximal respiratory capacity after the addition of respectively oligomycine (1 μM) and the FCCP protonophore (1 μM). Finally, rotenone (1 μM), an inhibitor of complex I, and antimycin (1 μM), inhibitor of complex III, were added to shut down completely the electron transport chain (ETC) function, revealing the non-mitochondrial respiration.

Generation of M368A hiPSC clone

The human induced pluripotent stem cell (hiPSC) line BIHi005-A (https://hpscreg.eu/cell-line/BIHi005-A) was used to generate an isogenic iPSC clone (BIHi005-A-39) with **M368A mutation** using a protocol previously described (41). In brief, small guide RNA (sgRNA) targeting the M_2 gene close to the mutation site to be corrected were designed using the http://crispor.tefor.net/ webpage and the sgRNA (5`- AGTCATCTTCACAATCTTGC-3`) were synthesized by Integrated DNA technologies (https://eu.idtdna.com). The donor ssODN template was designed to convert the ATG to GCT and was synthesized as an Ultramar DNA oligo by IDT. (5´-AAAAGTGACTCATGTACCCCAACTAATACCACCGTGGAGGTAGTGGGGTCTTCAGGTC AGAATGGAGATGAAAAGCAGAATATTGTAGCCCGCAAGATTGTGAAGGCTACTAAGCA GCCTGCAAAA-3´). The Ribonucleoprotein (RNP) complexes were prepared by incubating of 1.5µg Cas-9 protein and 360 ng gRNA for 10 minutes at room temperature. For delivery of RNPs and ssODN template, 10µl cell suspension containing Cas9 RNPs and ssODN and 1x105 cells were electroporated using the Neon transfection System (ThermoFisher Scientific). The electroporated cells were plated in one well of 6 well plate with StemFlex media (ThermoFisher Scientific) supplemented CloneR™ (Stemcell technologies). Three days after the transfection we analyzed the bulk population using the Sanger sequencing to estimate the editing efficiency. Thereafter, the automated single cell cloning of

the genome edited cell pool was performed as described in protocol (42). The clones were screened by SANGER sequencing. The positive confirmed clones were banked and characterized for pluripotency and karyotype stability as described in (43).

Briefly, for pluripotency assay, single cells were labelled with conjugated antibodies. Surface markers (SSEA1, SSEA4 and TRA1-60) staining was performed in unfixed cells by incubation with antibodies diluted in 0.5% BSA/PBS (10 min, 4 °C, dark). Intracellular markers (OCT3/4, NANOG) were stained by fixation/permeabilization solution (Miltenyi Biotec, 130-093-142) (30 min, 4 °C, dark) followed by antibody incubation in permeabilization buffer (Miltenyi Biotec) (30 min, 4 °C, dark). Analysis was done using the MACSQuant® AnalyzerVYB and FlowJo v10.4.

Briefly, for karyotype stability, genomic DNA was isolated using the DNeasy blood and tissue kit (Qiagen, Valencia, CA, United States) and samples were analyzed using the human Illumina OMNI-EXPRESS-8v1.6 BeadChip. First, the genotyping was analyzed using GenomeStudio 1 genotyping module (Illumina). Thereafter, KaryoStudio 1.3 (Illumina) was used to perform automatic normalization and to identify genomic aberrations utilizing settings to generate B-allele frequency and smoothened Log R ratio plots for detected regions. The stringency parameters used to detect copy number variations (CNVs) were set to 75 kb (loss), 100 kb (gain) and CN-LOH (loss of heterozygosity) regions larger than 3 MB.

Culture and handling of hiPSCs cells

hiPSCs were cultured on Geltrex (Thermo Fisher) coated plates using: Essential 8 medium (Thermo Fisher). The culture was routinely monitored for mycoplasma contamination using a PCR assay. 10 µM ROCK Inhibitor Y-27632 2HCl (Selleck Chemicals, #SEL-S1049) was added after cell splitting to promote survival. hiPSC cultures were kept in a humidified atmosphere of 5% CO2 at 37°C and 5% oxygen. hiPSCs were undirectedly differentiated to a mixture of three lineages (ectodermal, endodermal and mesodermal) by replacing Essential 8 medium with DMEM-F12 medium supplemented with 10% FBS for seven days. 10 µM ROCK Inhibitor Y-27632 2HCl (Selleck Chemicals) was added after cell splitting to promote survival.

Cell proliferation assay with HEK293 cells

$4x10^5$ HEK293 cells 24h after transfection and $4x10^5$ hPSCs were seeded respectively in T25 flask and pre-coated T25 flask, in culture medium with Atropine at final concentration of 100nM; the medium with Atropine was replaced every day. After 72h from transfection of the HEK293 and from seeding of the hiPSCs, the medium and the cells were collected and centrifuged, the pellet was resuspended in the same amount of medium for each pellet; an aliquots of the resuspension was mixed with the same amount of Trypan blue (ratio 1:1), 10 microliters were used for counting in a Neubauer chamber.

Fluorescence plate reader assays

HEK293 cells were grown on 6 well plates without coverslips, and, upon reaching 60-70% confluence, the cells were transfected using Effectene (Quiagen, Venlo Netherlands) according to the manufacturer's instructions. After 24 h the cells were split and transferred to 96 well (black plate) at a seeding density of 50,000 cells/well. The 96 well plate was pre-coated with Poly-D-Lysine for 30 min at RT. The medium was removed and each well was washed 3x with 100µl HBSS. The cells were finally analyzed by a fluorescence plate reader (Neo2, BioTek, Bad Friedrichshall) in HBSS.

Extracellular oxygen consumption

HEK293 cells 24h after transfection and hPSCs were harvested and seeded respectively in 96 multiwell black plate and pre-coated (Geltrex A1413302, Thermo Fisher) 96 multiwell black plate, $5x10^4$ cells for well; after incubation O/N at 37 °C and in 5% CO2, the cell culture medium was replaced by HBSS and the assay were performed according to the manufacturer protocols (abcam Extracellular Oxygen Consumption Assay).

Statistical analysis

Significance values reported in the graphs, in comparing tabulated values, were determined by a one-tailed Student t-test using Prism 9 (GraphPad Software), and significance values (p-values) are indicated according to the following legend: **** $p<0.0001$; *** $0.0001<p<0.001$; ** $0.001<p<0.01$;

* 0.01<p<0.05. p-values larger than 0.05 are deemed non-significant. Unless otherwise indicated, bar charts and scatter plots indicate average value with s.e.m.

References

1. A. C. Kruse, B. K. Kobilka, D. Gautam, P. M. Sexton, A. Christopoulos, J. Wess, Muscarinic acetylcholine receptors: novel opportunities for drug development. *Nat. Rev. Drug Discov.* **13**, 549-560 (2014).

2. A. D. Fryer, A. Christopoulos, N.M. Nathanson in *Handbook of Experimetal Pharmacology* Vol. 208 1-499 (2012).

3. F. Novi, M. Scarselli, G. U. Corsini, R. Maggio, The paired activation of the two components of the muscarinic M3 receptor dimer is required for induction of ERK1/2 phosphorylation. *J. Biol. Chem.* **279**, 7476-7486 (2004).

4. F. Novi, M. Scarselli, G. U. Corsini, R. Maggio, An unusual form of the association binding kinetics of N-[3H]methylscopolamine to the split muscarinic M2trunk/M2tail receptor. *J. Pharmacol. Exp. Ther.* **305**, 786-795 (2003).

5. R. J. Jackson, A. Kaminski, Internal initiation of translation in eukaryotes: the picornavirus paradigm and beyond. *RNA* **1**, 985-1000 (1995).

6. C. U. Hellen, P. Sarnow, Internal ribosome entry sites in eukaryotic mRNA molecules. *Genes. Dev.* **15**, 1593-1612 (2001).

7. D. Calebiro, V. O. Nikolaev, L. Persani, M. J. Lohse, Signaling by internalized G-protein coupled receptors. Trends in Pharmacol.l Sci. **31**, 221-228 (2010).

8. X. Zhang, A. V. Bedigian, W. Wang, U. S. Eggert, G protein-coupled receptors participate in cytokinesis. *Cytoskeleton (Hoboken)* **69**, 810-818 (2012).

9. E. Hebert-Chatelain, T. Desprez, R. Serrat, L. Bellocchio, E. Soria-Gomez, A. Busquets-Garcia, A. C. Pagano Zottola, A. Delamarre, A. Cannich, P. Vincent, M. Varilh, L. M. Robin, G. Terral, M. D. García-Fernández, M. Colavita, W. Mazie, F. Drago, N. Puente, L. Reguero, I. Elezgarai, J. W. Dupuy, D. Cota, M. L. Lopez-Rodriguez, G. Barreda-Gómez, F.Massa, P. Grandes, G. Bénard, G. Marsicano, A cannabinoid link between mitochondria and memory. *Nature* **539**, 555-559 (2016).

10. Y. Suofu, W. Li, F. G. Jean-Alphonse, J. Jia, N. K. Khattar, J. Li, S. V. Baranov, D. Leronni, A. C. Mihalik, Y. He, E. Cecon, V. L. Wehbi, J. Kim, B. E. Heath, O. V. Baranova, X. Wang, M. J. Gable, E. S. Kretz, G. Di Benedetto, T. R. Lezon, L. M. Ferrando, T. M. Larkin, M. Sullivan, S. Yablonska, J. Wang, M. B. Minnigh, G. Guillaumet, F. Suzenet, R. M. Richardson, S. M. Poloyac, D. B. Stolz, R. Jockers, P. A. Witt-Enderby, D. L. Carlisle, J. P. Vilardaga, R. M. Friedlander, Dual role of mitochondria in producing melatonin and driving GPCR signaling to block cytochrome c release. Proc. Nat. Acad. Sci. U.S.A **114**, E7997-E8006 (2017).

11. R. Maggio, I. Fasciani, M. Rossi, J. Di Gregorio, I. Pietrantoni, V. Puca, V. Flati, M. Scarselli, Variants of G protein-coupled receptors: a reappraisal of their role in receptor regulation. *Biochem. Soc. Trans.* **44**, 589-594 (2016).

12. R. Maggio, Z. Vogel, J. Wess, Reconstitution of functional muscarinic receptors by co-expression of amino- and carboxyl-terminal receptor fragments. *FEBS Lett.* **319**, 195-200 (1993).

13. P.S Park, J. W. Wells, Monomers and oligomers of the M2 muscarinic cholinergic receptorpurified from Sf9 cells. *Biochemistry* **42**, 12960-12971 (2003).

14. M. Bathe-Peters, P. Gmach, P. Annibale, P., M.J. Lohse, Linescan microscopy data to extract diffusion coefficient of a fluorescent species using a commercial confocal microscope. *Data Brief.* **29**, 105063, (2020).

15. C. Dong, C. M. Filipeanu, M.T. Duvernay, G. Wu, Regulation of G protein-coupled receptor export trafficking. *Biochim. Biophys. Acta* **1768**, 853-870 (2007).

16. D. Kamiyama, S. Sekine, B. Barsi-Rhyne, J. Hu, B. Chen, L. A. Gilbert, H. Ishikawa, M. D. Leonetti, W. F. Marshall, J. S. Weissman , B. Huang, Versatile protein tagging in cells with split fluorescent protein. *Nat. Commun.* **7**, 11046 (2016).

17. L. Bonfili, V. Cecarini, M. Cuccioloni, M. Angeletti, V. Flati, G. Corsetti, E. Pasini, F. S. Dioguardi, A. M. Eleuteri, Essential amino acid mixtures drive cancer cells to apoptosis through proteasome inhibition and autophagy activation. *FEBS J.* **284**, 1726-1737 (2017).

18. N. Thakor, M. Holcik, IRES-mediated translation of cellular messenger RNA operates in eIF2alpha- independent manner during stress. *Nucleic Acids Res* **40**, 541-552, (2012).

19. M. Holcik, N. Sonenberg, Translational control in stress and apoptosis. *Nat. Rev. Mol. Cell. Biol.* **6**, 318-327 (2005).

20. L. E. Newman, C. Schiavon, R. A. Kahn, Plasmids for variable expression of proteins targeted to the mitochondrial matrix or intermembrane space. *Cell. Logist.* **6**, e1247939, (2016).

21. T. Ishizuka, A. Ozawa, M. Katsuura, S. Nomura, Y. Satoh, Effects of muscarinic acetylcholine receptor stimulation on the differentiation of mouse induced pluripotent stem cells into neural progenitor cells. *Clin. Exp. Pharmacol. Physiol.* **45**, 1198-1205 (2018).

22. M. Hoogduijn, A. Cheng, P. G. Genever, Functional nicotinic and muscarinic receptors on mesenchymal stem cells. *Stem. Cells Dev.* **18**, 103-112 (2009).

23. Z. Y. Weinberg, M. A. Puthenveedu, Regulation of G protein-coupled receptor signaling by plasma membrane organization and endocytosis. *Traffic* **20**, 121-129 (2019).

24. Y. I. Jong, S. K. Harmon, K. L. O'Malley, GPCR signalling from within the cell. *Br. J. Pharmacol.* **175**, 4026-4035 (2018).

25 G. Benard, F. Massa, N. Puente, J. Lourenço, L. Bellocchio, E. Soria-Gómez, I. Matias, A. Delamarre, M. Metna-Laurent, A. Cannich, E. Hebert-Chatelain, C. Mulle, S. Ortega-Gutiérrez, M. Martín-Fontecha, M. Klugmann, S. Guggenhuber, B. Lutz, J. Gertsch, F. Chaouloff, M. L. López-Rodríguez, P. Grandes, R. Rossignol, G. Marsicano, Mitochondrial CB(1) receptors regulate neuronal energy metabolism. *Nat. Neurosci.* **15**, 558-564 (2012).

26. K. Lefkimmiatis, D. Leronni, A. M. Hofer, The inner and outer compartments of mitochondria are sites of distinct cAMP/PKA signaling dynamics. *J. Cell. Biol.* **202**, 453-462 (2013).

27. M. Marti-Solano, S. E. Crilly, D. Malinverni, C. Munk, M. Harris, A. Pearce, T. Quon, A. E. Mackenzie, X. Wang, J. Peng, A. B. Tobin, G. Ladds, G. Milligan, D. E. Gloriam, M. A. Puthenveedu, M. Madan Babu, Combinatorial expression of GPCR isoforms affects signalling and drug responses. *Nature* **587**, 650-656 (2020).

28. S.van Heesch, F. Witte, V. Schneider-Lunitz , J. F. Schulz, E. Adami, A. B. Faber, M. Kirchner, H. Maatz, S. Blachut, C. Sandmann, M. Kanda, C. L. Worth, S. Schafer, L. Calviello, R. Merriott, G. Patone, O. Hummel, E. Wyler, B. Obermayer, M. B. Mücke, E. L. Lindberg, F. Trnka, S. Memczak, M. Schilling, L. E. Felkin, P. J. R. Barton, N. M. Quaife, K. Vanezis, S. Diecke, M. Mukai, N. Mah, S. Oh, A. Kurtz, C. Schramm, D. Schwinge, M. Sebode, M. Harakalova, F. W. Asselbergs, A. Vink, R.A. de Weger, S. Viswanathan, A. A. Widjaja, A. Gärtner-Rommel, H. Milting, C. Dos Remedios, C. Knosalla, P. Mertins, M. Landthaler, M. Vingron, W. A. Linke, J. G. Seidman, C. E. Seidman, N. Rajewsky, U.

Ohler, S. A. Cook, N. Hubner, The Translational Landscape of the Human Heart. *Cell* **178**, 242-260 e229 (2019).

29. T. V. Pestova, I. N. Shatsky, C. U. Hellen, Functional dissection of eukaryotic initiation factor 4F: the 4A subunit and the central domain of the 4G subunit are sufficient to mediate internal entry of 43S preinitiation complexes. *Mol. Cell. Biol.* **16**, 6870-6878 (1996).

30. E. Jan, P. Sarnow, Factorless ribosome assembly on the internal ribosome entry site of cricket paralysis virus. *J. Mol. Biol.* **324**, 889-902 (2002).

31. K.D. Fitzgerald, B. L. Semler, Bridging IRES elements in mRNAs to the eukaryotic translation apparatus. *Biochim. Biophys. Acta* **1789**, 518-528 (2009).

32. N. T. Ingolia, J. A. Hussmann, J. S. Weissman, Ribosome Profiling: Global Views of Translation. *Cold. Spring. Harb. Perspect. Biol.* **11,** (5):a032698 (2019).

33. J. Zhang, E. Nuebel, G. Q. Daley, C. M. Koehler, M. A. Teitell, Metabolic regulation in pluripotent stem cells during reprogramming and self-renewal. *Cell Stem Cell.* **11**, 589-595 (2012).

34. C. Guo, L. Sun, X. Chen, D. Zhang, Oxidative stress, mitochondrial damage and neurodegenerative diseases. *Neural. Regen. Res.* **8**, 2003-2014 (2013).

35. P. Kritsiligkou, A. Chatzi, G. Charalampous, A. Mironov Jr, C. M. Grant, K. Tokatlidis, Unconventional Targeting of a Thiol Peroxidase to the Mitochondrial Intermembrane Space Facilitates Oxidative Protein Folding. *Cell Rep.* **18**, 2729-2741 (2017).

36. T. I. Bonner, N. J. Buckley, A. C. Young, M. R. Brann, Identification of a family of muscarinic acetylcholine receptor genes. *Science* **237**, 527-532 (1987).

37. M. Kozak, Constraints on reinitiation of translation in mammals. *Nucleic Acids Res.* **29**, 5226-5232 (2001).

38. M. Kozak, Circumstances and mechanisms of inhibition of translation by secondary structure in eucaryotic mRNAs. *Mol. Cell Biol.* **9**, 5134-5142 (1989).

39. E. M. M. Manders, F. J. Verbeek, J. A. Aten, Measurement of Colocalization of Objects in Dual-Color Confocal Images. *J. Microsc. (Oxford)* **169**, 375-382 (1993).

40. E. M. M. Manders, J. Stap, G. J. Brakenhoff, R. Vandriel, J. A. Aten, Dynamics of 3-Dimensional Replication Patterns during the S-Phase, Analyzed by Double Labeling of DNA and Confocal Microscopy. *J. Cell Sci.* **103**, 857-862 (1992).

41. C. D. Richardson, G. J. Ray, M. A. DeWitt, G. L. Curie, J. E. Corn, Enhancing homology-directed genome editing by catalytically active and inactive CRISPR-Cas9 using asymmetric donor DNA. *Nat. Biotechnol.* **34**, 339-344 (2016).

42. V. F. Vallone, N. S. Telugu, I. Fischer, D. Miller, S. Schommer, S. Diecke, H. Stachelscheid, Methods for Automated Single Cell Isolation and Sub-Cloning of Human Pluripotent Stem Cells. *Curr. Protoc. Stem Cell Biol.* **55,** (1):e123 (2020).

43. E. Metzler, N. Telugu, S. Diecke, S. Spuler, H. Escobar, Generation of two human induced pluripotent stem cell lines derived from myoblasts (MDCi014-A) and from peripheral blood mononuclear cells (MDCi014-B) from the same donor. *Stem Cell Res.* **48**, 101998 (2020).

44. R. Maggio, P. Barbier, A. Colelli, F. Salvadori, G. Demontis, G. U. Corsini, G protein-linked receptors: pharmacological evidence for the formation of heterodimers. *J Pharmacol Exp Ther* **291**, 251-257 (1999).

45. S. Rauth, K. Y. Song, D. Ayares, L. Wallace, P. D. Moore, R. Kucherlapati, Transfection and homologous recombination involving single-stranded DNA substrates in mammalian cells and nuclear extracts. *Proc. Natl. Acad. Sci. U.S.A.* **83**, 5587-5591 (1986).

46. F. Schueren, T. Lingner, R. George, J. Hofhuis, C. Dickel, J. Gärtner, S. Thoms, Peroxisomal lactate dehydrogenase is generated by translational readthrough in mammals. *Elife* **3**, e03640 (2014).

47. G. Loughran, M.Y. Chou, I. P. Ivanov, I. Jungreis, M. Kellis, A. M. Kiran, P. V. Baranov, J. F. Atkins, Evidence of efficient stop codon readthrough in four mammalian genes. *Nucleic Acids Res* **42** (2014).

48. Powell, M. L., Napthine, S., Jackson, R. J., Brierley, I. & Brown, T. D. Characterization of the termination-reinitiation strategy employed in the expression of influenza B virus BM2 protein. *RNA* **14**, 2394-2406, doi:10.1261/rna.1231008 (2008).

49. D. Wessel, U. I. Flugge, A method for the quantitative recovery of protein in dilute solution in the presence of detergents and lipids. *Anal. Biochem.* **138**, 141-143 (1984).

50. J. Rappsilber, Y. Ishihama, M. Mann, Stop and go extraction tips for matrix-assisted laser desorption/ionization, nanoelectrospray, and LC/MS sample pretreatment in proteomics. *Anal. Chem.* **75**, 663-670 (2003).

51. S. Gessulat, T. Schmidt, D.P. Zolg, P. Samaras, K. Schnatbaum, J. Zerweck, T. Knaute, J. Rechenberger, B. Delanghe, A. Huhmer, U. Reimer, H.C. Ehrlich, S. Aiche, B. Kuster, M. Wilhelm, Prosit: proteome-wide prediction of peptide tandem mass spectra by deep learning. *Nat Methods* **16**, 509-518 (2019).

52. B. MacLean, D. M. Tomazela, N. Shulman, M. Chambers, G. L. Finney, B. Frewen, R. Kern, D. L. Tabb, D. C. Liebler, M. J. MacCoss, Skyline: an open source document editor for creating and analyzing targeted proteomics experiments. *Bioinformatics* **26**, 966-968 (2010).

53. U. H. Toprak, L. C. Gillet, A. Maiolica, P. Navarro, A. Leitner, R. Aebersold, Conserved peptide fragmentation as a benchmarking tool for mass spectrometers and a discriminating feature for targeted proteomics. *Mol Cell Proteomics* **13**, 2056-2071 (2014).

54. J. Cox, M. Mann, MaxQuant enables high peptide identification rates, individualized p.p.b.-range mass accuracies and proteome-wide protein quantification. *Nat. Biotechnol.* **26**, 1367-1372 (2008).

55. S. E. Calvo, K. R. Clauser, V. K. Mootha, MitoCarta2.0: an updated inventory of mammalian mitochondrial proteins. *Nucleic Acids Res.* **44**, D1251-1257 (2016).

56. Y. Perez-Riverol, A. Csordas, J. Bai, M. Bernal-Llinares, S. Hewapathirana, D. J. Kundu, A. Inuganti, J. Griss, G. Mayer, M. Eisenacher, E. Pérez, J. Uszkoreit, J. Pfeuffer, T. Sachsenberg, S. Yilmaz, S. Tiwary, J. Cox, E. Audain, M. Walzer, A. F. Jarnuczak, T. Ternent, A. Brazma, J. A. Vizcaíno The PRIDE database and related tools and resources in 2019: improving support for quantification data. *Nucleic Acids Res.* **47**, D442-D450 (2019).

57. J. Zhang, E. Nuebel, D. R. R. Wisidagama, K. Setoguchi, J. S. Hong, C. M. Van Horn, S. S. Imam, L. Vergnes, C. S. Malone, C. M. Koehler, M. A. Teitell, Measuring energy metabolism in cultured cells, including human pluripotent stem cells and differentiated cells. *Nat Protoc* **7**, 1068-1085 (2012).

Acknowledgments

We are grateful to Dr. Marco Marcia (EMBL) for insightful discussion.

Funding:

European Union's Horizon2020 Marie Skłodowska-Curie Actions (MSCA)

Program under Grant Agreement 641833 (ONCORNET).

Author contributions:

Conduced primary experiments: PA, FP, IF, ZW, MR, IP, RE, HZ, UZ, MET, JDG, SS, ART, SA

Contributed to the experimental data: MG, CP, GA, FM, BP, AR

Contributed tools and reagents: NT and SD

Contributed to experimental design and assisted in writing paper: PA, IP, IF, MR, UZ, AT, KT, VF, FA, FG, MS

Conceived and lead the study, and wrote the paper: PA, MJL and RM

Competing interests:

The authors declare that they have no conflicts of interest with the contents of this article.

Data and materials availability:

Source data are provided with this manuscript.

Figures and Tables

Table 1. Radioligand binding and activation properties of M_2 receptor mutants. Binding properties and inhibition of forskolin stimulated adenylyl cyclase by M_2, M_2stop228 and the co-transfected M_2trunk(1-283)/M_2tail(M-281-466) and M_2trunk(1-228)/M_2tail(368-466). Untransfected COS-7 cells did not show any [^{3}H]NMS specific binding. N.B. = no specific [^{3}H]NMS binding. Data are averages with s.e.m.

Binding data				Adenylyl cyclase inhibition assay	
Receptor	Bmax (fmol/mg)	[^{3}H]NMS KD (pM)	Carbachol IC50 (μM)	Carbachol EC50 (μM)	Maximum inhibition of forskolin stimulated cAMP accumulation (%)
M_2	980 ± 60	62 ± 7	2.1 ± 0.6	0.04 ± 0.01	53 ± 5
M_2trunk(1-283)	N.B.				

M_2trunk(1-228)	N.B.				
M_2stop228	45 ± 2	70 ± 10	1.8 ± 0.4	0.13 ± 0.02	27 ± 3
M_2trunk(1-283) +M_2tail(M-281-466)	480 ± 20	79 ± 10	0.7 ± 0.2	0.15 ± 0.03	37 ± 4
M_2trunk(1-228) +M_2tail(368-466)	70 ± 10	72 ± 8	0.6 ± 0.2	0.17 ± 0.03	29 ± 4

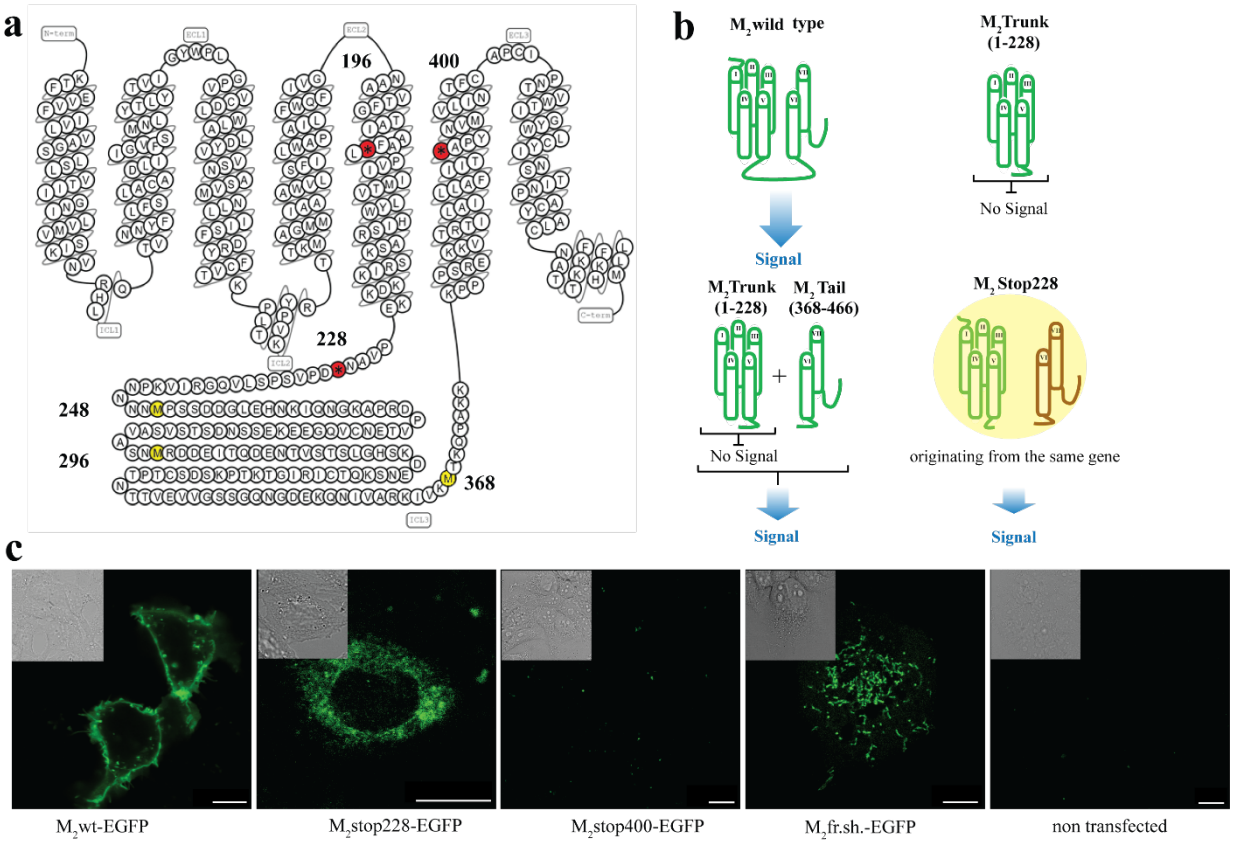

Fig. 1. Mutations of the M_2 receptor confer unexpected functional and localization properties. **a**, Snake-like plot of the human muscarinic M_2 receptor: in red are indicated the aminoacids substituted with stop codons in the mutants: M_2stop196, M_2stop228 and M_2stop400 (**Fig. S1**). The three in-frame methionines of the i3 loop, 248, 296 and 368, are highlighted in yellow; the translation of the C-terminal fragment starts from methionine 368. **b**, Schematic representation of the gene products that reach the plasma membrane of the wild type M_2, M_2trunk, M_2trunk and M_2tail and M_2stop228 (**Fig. S1**). The M_2trunk and M_2tail genes generate the respective protein fragments that, only when co-transfected together, are able to form functional receptor complexes capable to bind ligands. The M_2stop228 gene mutant generates both M_2trunk (in green), when translation starts from the cap site, and M_2tail (in brown) when

translation is cap-independent driven. This makes it likely that the truncated fragment of the M_2stop228 receptor may act as a chaperon driving part of the C-terminal-M_2 fragment to the plasma membrane, as supported by the binding and functional data shown by the co-transfection of M_2trunk(1-228) with M_2tail(368-466) (**Table 1**). **c**, Fluorescence micrographs of HEK293 cells respectively expressing M_2-EGFP, M_2stop228-EGFP, M_2fr.sh.-EGFP and M_2stop400-EGFP, together with an untransfected control. Imaging settings are the same for the five images, whereas contrast was adjusted to improve visualization. In the untransfected cells and stop400 panels, the contrast was set to 0. Insets display DIC image of the same field of view (scale bars 10 µm).

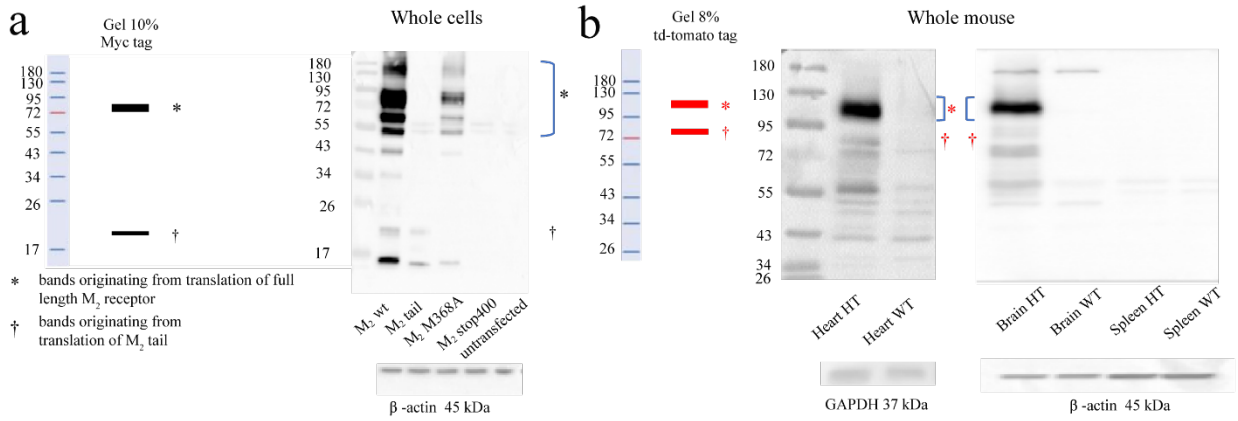

Fig. 2. Western blot of tagged M_2 receptor mutants in HEK293 cells and in tdtomato knock-in mice. a, left Graphical guide of the fragments observed on the gel when using myc-tag. **right**, M_2-myc, M_2tail(368-466)-myc, M_2M368A-myc and M_2stop400-myc were transiently transfected in HEK293 cells and immunodetected via antimyc primary antibody, together with an untransfected control. Loading control normalization was performed vs β-actin **b**, **left** Graphical guide of the fragments observed on the gels when using the tdtomato tag. **right**, Western blot from tissue preparations originating from the indicated organs of M_2-tdtomato knock-in mice (HT) and wild-type animals (WT). Immunodetection was performed using an anti-tdtomato primary antibody. Loading control normalization was performed using GAPDH in the heart, and β-actin in the brain and spleen.

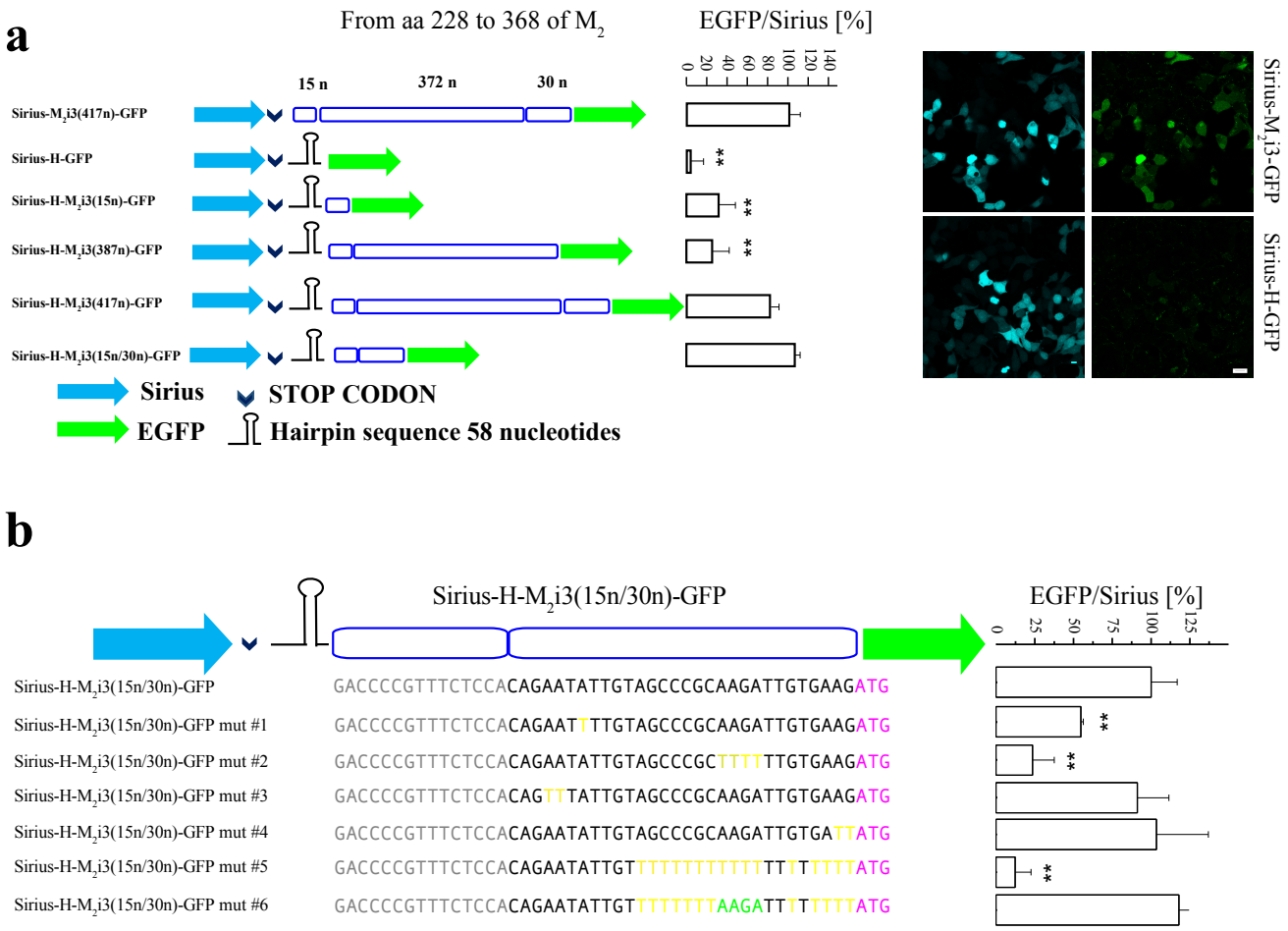

Fig. 3. Fluorescence assay of cap-independent translation of EGFP driven by the i3 loop mutants of the muscarinic M_2 receptor. a, **left** Schematic representation of bicistronic plasmids bearing the M_2 i3 loop between the coding regions of the Sirius and EGFP fluorescent proteins. A guanine nucleotide was originally inserted before the EGFP in the plasmid Sirius-H-EGFP in order to maintain in frame the sequences of the two fluorescent proteins. In all the other plasmids the sequence of the two fluorescent proteins is not in frame. Fifteen nucleotides derived from the M_2 i3 loop were inserted between the end of Sirius and the hairpin loop, in order to allow the easy scanning of the ribosome across the stop codon. **right**, Relative fluorescence of EGFP compared to Sirius, highlighting the efficiency of cap-independent translation for the control Sirius-M_3i3(417n)-EGFP and the six mutants. The insert shows the difference in the green fluorescence between two of the mutants. Significance values reported in the graphs were determined by a one-tailed Student t-test, p-values: ** $0.001<p<0.01$. **b**, **left** Mutations of the bicistronic Sirius-H-M_2i3(15n/30n)-EGFP plasmids in the region of the M_2 i3 loop from nucleotides 1972 to 2001, in yellow are the modified nucleotides. In Sirius-H-M_2i3(15n/30n)mut#6-EGFP the four nucleotides in green (AAGA) were reinserted in the stretch of 20 T of Sirius-H-M_2i3(15n/30n)mut#5-EGFP. **right** Relative fluorescence of EGFP compared to Sirius, highlighting the efficiency of cap-independent translation for the control Sirius-H-M_2i3(15n/30n)-EGFP and the six mutants illustrated. Significance ($p < 0.01$) was calculated in **a** against Sirius-M_2i3(417n)-EGFP and in **b** against Sirius-H- M_2i3(15n/30n)-EGFP. Error bars are s.e.m. Significance values reported in the graphs were determined by a one-tailed Student t-test, p-values: ** $0.001<p<0.01$.

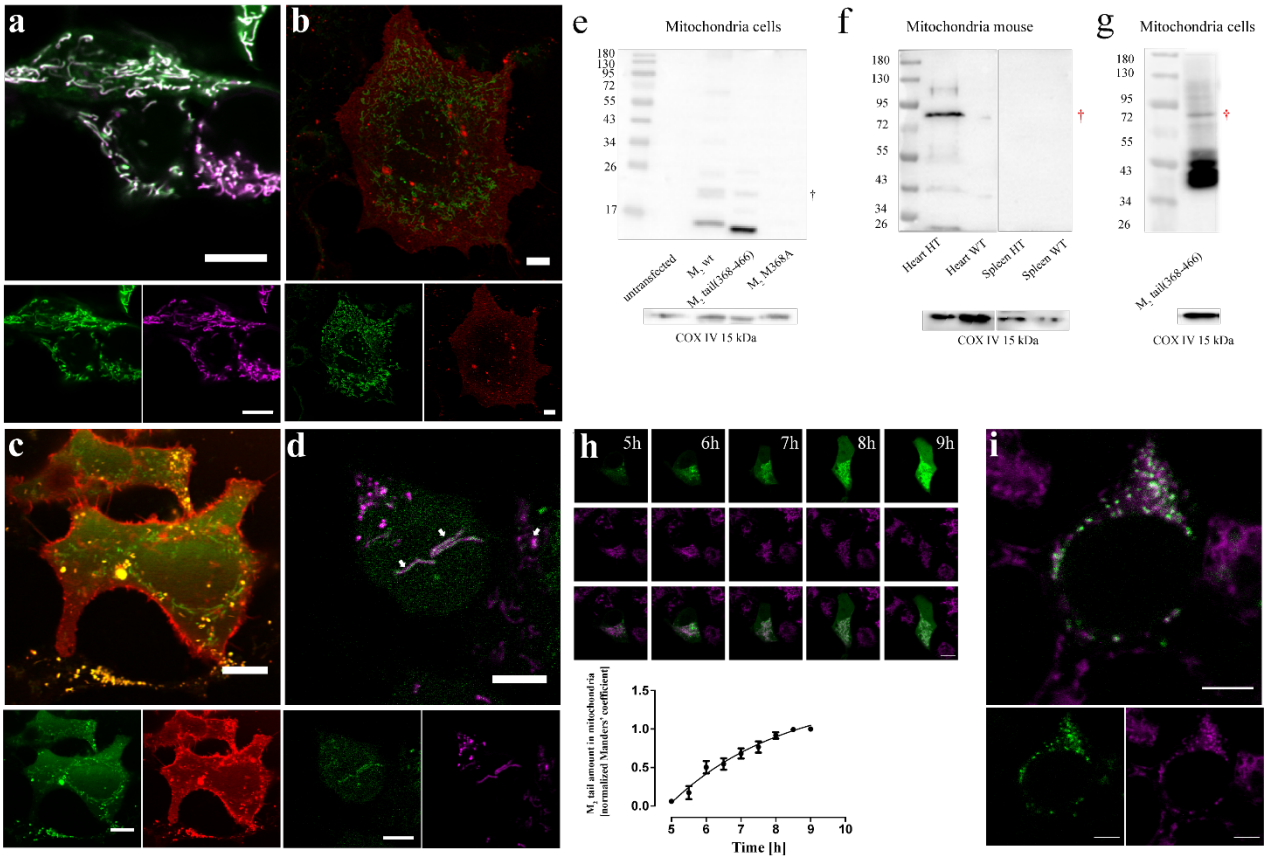

Fig. 4. Localization of fluorescently labeled M_2 mutant constructs: microscopy and western blots analysis. a, Colocalization of M_2tail(368-466)-EGFP (green) together with the mitochondrial targeted dye Mitotracker (magenta) in HEK293 cells. Separate spectral channels are displayed below. **b**, Co-expression of M_2tail(368-466)-EGFP (green) and wild type M_2-mRuby2 (red) in HEK293 cells. Separate spectral channels are displayed below. **c**, Cellular localization of the construct M_2-mRuby2-STOP-M_2-i3-tail-EGFP in HEK293 cells. Expression of the M_2tail(368-466)-EGFP (green) after the STOP codon is an indicator of the endogenous IRES activity. While M_2-mRuby2 localizes correctly and predominantly to the cell plasma membrane, M_2tail(368-466)-EGFP localizes in the cytosol as well as, strongly, to the cell mitochondria. Separate spectral channels are displayed below. **d**, M_2-fr.sh.-EGFP (green) expressed in conjunction with Mitotracker (magenta). The EGFP is expressed despite the creation of an in-frame stop after M368, confirming endogenous cap-independent translation of the M_2tail(368-466). Arrows indicate areas of colocalization with the mitochondria. Separate spectral channels are displayed below. **e**, Western blot (10% TRIS-Glycine PAA gel) of mitochondria purified from Hek293 cells transfected with the M_2-Myc, M_2tail(368-466)-Myc, M_2M368A-Myc, together with an untransfected control are blotted using an anti-myc antibody. Loading control was verified by immunoblotting COXIV. **f**, Western blot (8% TRIS-Glycine PAA gel) of mitochondria purified from tissue preparations originating from the indicated organs of M_2-tdtomato knock-in mice (HT) and wild-type animals (WT), detected using an anti-tdtomato antibody. Please note that the band at 80kDa is aspecific, and is more prominent in the WT lane due to higher loading. **g**, Western blot (8% TRIS-Glycine PAA gel) of mitochondria purified from HEK293 cells transfected with the M_2tail(368-466)-tdtomato, together with an untransfected control. Mitochondrial proteins were blotted using an anti-tdtomato antibody. Loading control was verified by detecting the 15 kDa mitochondrial

matrix protein Cox-IV. **h** Time course of M_2tail(368-466)-EGFP import in the mitochondria of a HEK293 cell over a 4h interval, starting 5h after cell transfection, as indicated. Panels, from top to bottom show M_2tail(368-466)-EGFP (green), Mitotracker (magenta) and overlay displaying increasing colocalization over time. Chart at the bottom quantifies colocalization of the M_2tail(368-466)-EGFP in the mitochondria by calculating the Manders Coefficients (n=7 cells, from 3 independent transfections, error bars are s.e.m.) (See **Methods**). **i**, Detail of a HEK293 cell expressing the M_2-GFP11 construct together with pmito-GFP1-10. The M_2-GFP11 was sequentially transfected 24 h after the pmito-GFP1-10 (see **Methods**) Magenta overlay indicates mitotracker. White signal in the overlay indicates M_2tail(368-466) trafficking to the organelle. All confocal micrographs were obtained by sequential imaging using 488 nm excitation and detection in the 520-600 nm (EGFP), 561 nm excitation and detection in the 580-650 nm (mRuby2) and at 633 nm and detected in the 650-700 nm range (Mitotracker) using HyD detectors in Photon Counting Mode. Scale bars are 10 µm throughout.

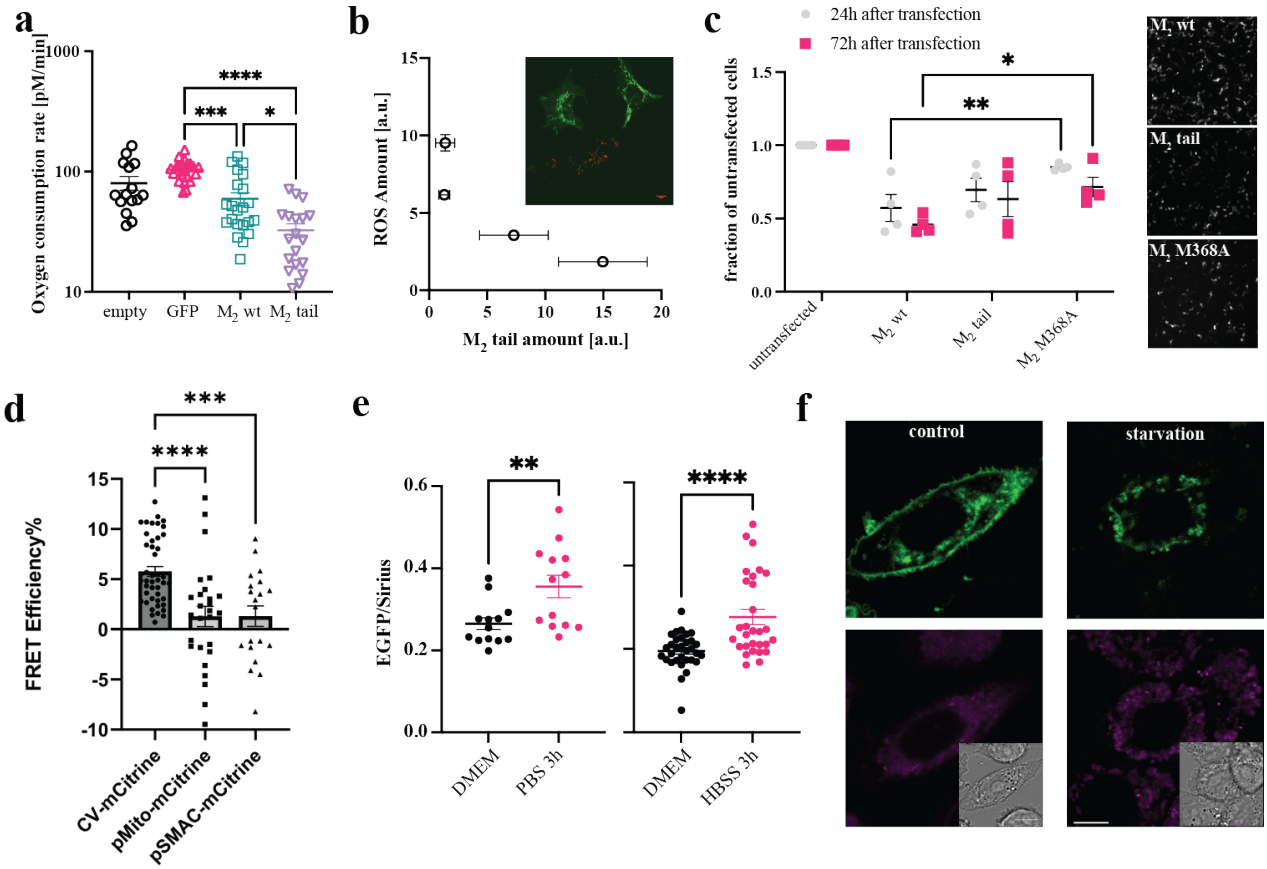

Fig. 5. Effects of M_2 mutants on mitochondrial function and cell metabolism in transfected HEK293 cells. a, Basal oxygen consumption upon HEK293 cell stress -following starvation- measured by a Seahorse assay at a constant temperature of 37 °C. Significance values reported in the graphs were determined by a one-tailed Student t-test, p-values: **** $p<0.0001$; *** $0.0001<p<0.001$;* $0.01<p<0.05$. **b**, Localization of M_2tail(368-466)-EGFP in HEK293

(green) cells stained with a marker for reactive oxygen species (Cell Rox Deep Red, ThermoFisher). Relationship between green (M_2tail abundance) vs red (amount of ROS produced) fluorescence intensities measured from regions of the mitochondrial network. The data were binned in four groups as a function of the amplitude of Cell Rox Deep Red signal (0-2.5, 2.5-5. 5-7.5 and 7.5-10 intensity counts). **c**, Cell viability assay performed on HEK293 cells transfected with M_2, M_2tail(368-466) and M_2(M368A), compared to an untransfected control. Cells were counted 24h and 72h after transfection in T-25 flasks, exposed throughout to 100 nM atropine. The experiments were performed in two biological replicates, each with two technical replicates. Transfection efficiency (to the right of the chart) was monitored thanks to the mRuby2 fluorescent reporter within a bicistronic cassette within each vector (see **Methods**). Significance values reported in the graphs were determined by a one-tailed Student t-test, p-values: ** $0.001<p<0.01$; * $0.01<p<0.05$. **d**, FRET efficiency plot of the interaction between M_2tail(368-466)-mTurquoise2 and F_0F_1ATP Synthetase (CV-mCitrine), COX8a-mCitrine and SMAC-mCitrine, as determined by acceptor photobleaching measurement in a confocal microscope. Each dot represents a ROI within a cell. At least 3 cells from two separate transfections were imaged for each pair. **e**, 96-well plate reader measurement of the increase of EGFP fluorescence relative to Sirius in COS-7 cells transfected with the bicistronic Sirius-M_2i3(417n)-EGFP plasmid and starved for three hours respectively in PBS (left panel) (n= 3 transfections, 16 wells) and HBSS (right panel) (n=1 transfection, 16 wells). Significance values reported in the graphs were determined by a one-tailed Student t-test, p-values: **** $p<0.0001$; ** $0.001<p<0.01$. **f**, HEK293 cells were sequentially transfected with pMito-GFP1-10 (24h) and M_2-GFP11 (8h, of which 6h under starvation conditions). (left panels) HEK293 cells grown in full culture medium and (right panels) HEK293 cells starved for 6 h after transfection of M_2-GFP11.Shown are EGFP fluorescence (top, with DIC inset) and Mitotracker (bottom).

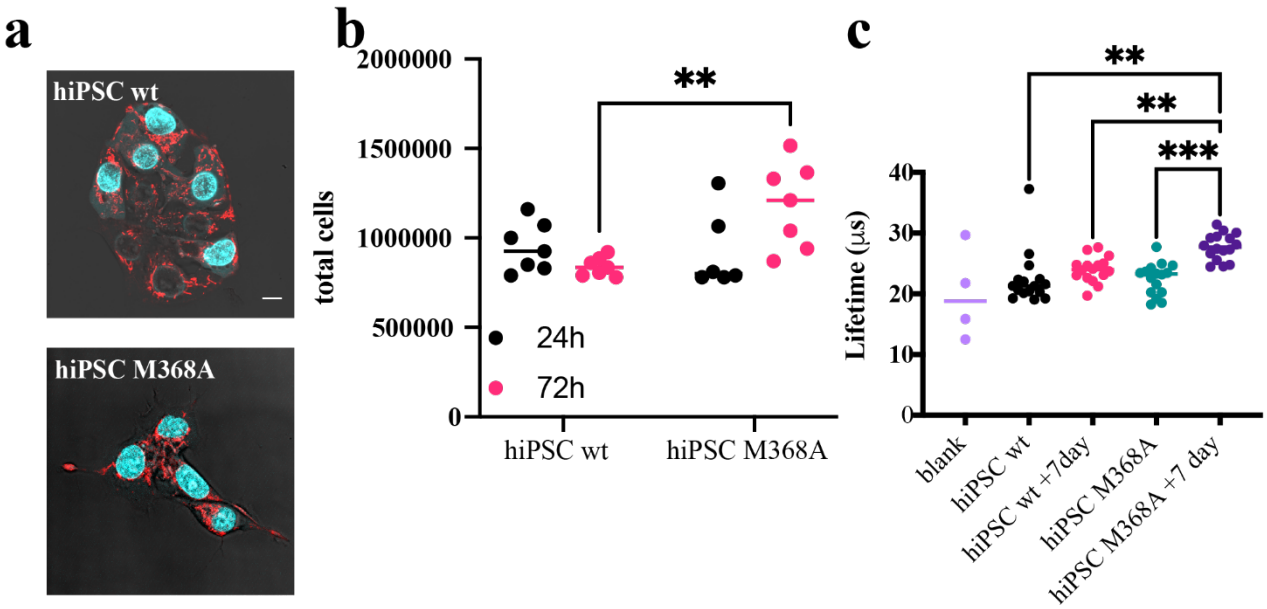

Fig. 6. Effects of M368A mutation on cell metabolism in hiPSCs a, Confocal micrographs of wt hiPSCs (left) and those harboring the M368A mutation within the M_2 gene (right), stained with DAPI (cyan) and Mitotracker (red). **b**, Cell proliferation assay performed for wt hiPSCs and M368A hiPSCs grown in T25 flasks. Cells were counted 24h and 72h after seeding. Significance values reported in the graphs were determined by a one-tailed Student t-test, p-values: ** $0.001<p<0.01$. **c**, Extracellular oxygen consumption assay, performed on wt and M368A hiPSCs, prior to and after 7 days undirected differentiation. The lifetime of a commercial dye increases as oxygen in the medium is progressively

consumed by the cells. The data displayed are collected after 60 minutes incubation. Significance values reported in the graphs were determined by a one-tailed Student t-test, p-values: *** 0.0001<p<0.001; ** 0.001<p<0.01.

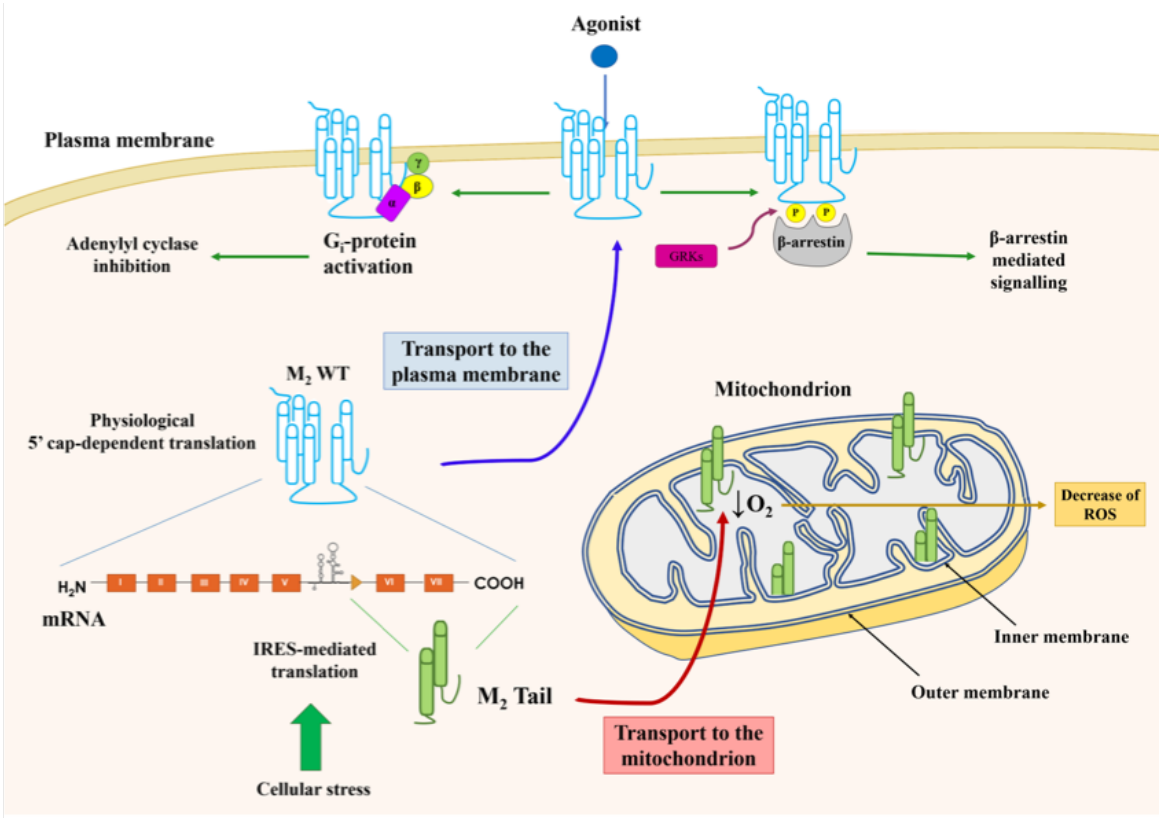

Fig. 7. Schematic representation of the wild type M_2 receptor gene products, their destination in the cell and their function. The M_2 receptor gene give rise to two different transcripts: when translation starts from the canonical cap site the wild type M_2 receptor is generated (in blue). When translation is driven by the internal ribosome entry site (IRES) the C-terminal fragment M_2tail is generated (in green). The two proteins are then sorted in two different cell compartments where they play completely different roles: the M_2 receptor is transported to the plasma membrane where it functions as a G protein-coupled neurotransmitter receptor and inhibits the adenylyl cyclase and β-arrestin mediated signalling. The M_2tail is instead transported in the mitochondria where it inhibits mitochondrial respiration and reduces ROS formation. IRES driven M_2tail translation is probably stimulated in para-physiological and pathological conditions and might have a protective role in cells expressing muscarinic M_2 receptors.